



1 Monthly element/Ca trends and inter chamber variability in two planktic Foraminifera
2 species: *Globigerinoides ruber albus* and *Turborotalita clarkei* from a hypersaline
3 oligotrophic sea

4
5
6 Noy Levy^{1,2}, Adi Torfstein^{1,3}, Ralf Schiebel², Natalie Chernihovsky^{1,3}, Klaus Peter
7 Jochum² , Ulrike Weis², Brigitte Stoll², Gerald H. Haug^{2,4}

8
9 1) The Fredy & Nadine Herrmann Institute of Earth Sciences, Hebrew University of
10 Jerusalem, Jerusalem 91904, Israel.

11 2) Max Planck Institute for Chemistry, Hahn-Meitner-Weg 1, 55128 Mainz, Germany.

12 3) Interuniversity Institute for Marine Sciences, Eilat 88103, Israel.

13 4) Department of Earth Sciences, ETH Zurich, Sonneggstrasse 5, 8092 Zurich, Switzerland

14  Deceased, November 9, 2024

15
16 Correspondence to: Noy Levy (noy.levy2@mail.huji.ac.il)

17
18
19 Abstract

20
21 Environmental and biological factors influence the trace element composition (element/Ca) of
22 planktic foraminifer shells. Consequently, the element/Ca measured in these shells (tests) are
23 utilized as proxies to reconstruct past oceanic and climatic conditions. As single shell analyses
24 are increasingly used in paleoceanographic research it is important to understand how proxy
25 systematics change between species, individuals of the same species in a given population, and
26 among chambers of a single individual during its life cycle. Here we present a time series of
27 the chemical composition of planktic foraminifers retrieved using sediment traps between June
28 2014 and June 2015 at the northern part of the Gulf of Aqaba (aka Gulf of Eilat). Laser ablation
29 ICP-MS element/Ca measurements were performed on single shells and chambers of
30 *Globigerinoides ruber albus* and *Turborotalita clarkei*, collected monthly from five water
31 depths (120 m, 220 m, 350 m, 450 m, and 570 m). Sediment trap samples were paired with
32 corresponding data on water column hydrography and chemistry. Pooled means of measured
33 element/Ca display species-specific and element-specific behavior, with generally higher



34 values for *T. clarkei* phenotypes ('big' and 'encrusted') in comparison to *G. ruber albus*. Some
35 element/Ca values measured in water column specimens, such as Al/Ca, vary significantly
36 from core-top specimens. A unique finding is a prominent increase in element/Ca around
37 March-April 2015, during maximum water column mixing, mostly apparent in *T. clarkei* and
38 to a lesser extent in *G. ruber albus*. This spring element/Ca increase is observed in most
39 measured elements and is further associated with an increase in inter-chamber variability
40 (ICV). Inter-chamber element/Ca patterns show element enrichment/depletion in the most
41 recently precipitated (final, F0) chamber in comparison to the older chambers (penultimate (F-
42 1), antepenultimate (F-2), etc.). Element/Ca in F0 may also be less sensitive to surrounding
43 environmental conditions. For example, the Mg/Ca of the F-1 and F-2 chambers of *G. ruber*
44 *albus* display a positive relationship with mixed layer temperatures while F0 does not. To
45 overcome this effect, we suggest using pooled means from non-F0 fractions as environmental
46 records and paleo proxies.

47 These results highlight the complexity of proxy systematics that rises from the variability in
48 element/Ca measured among different species and between chambers, caused by ecological
49 conditions and other processes in the water column including physical, chemical, and
50 biological effects.

51

52 1. Introduction

53 1.1 Planktic foraminifera as traces of the past environment

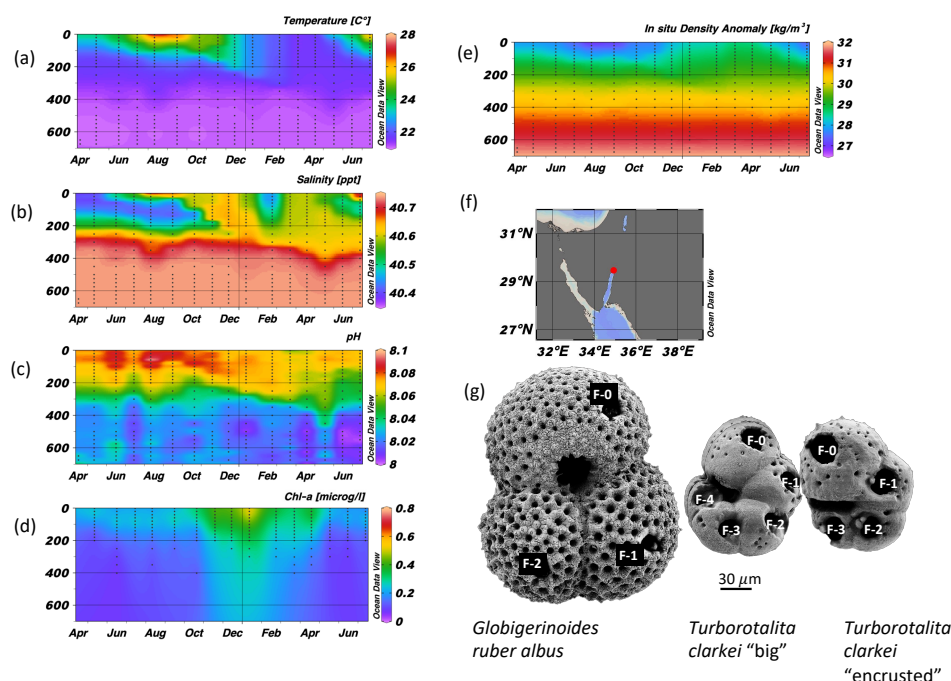
54 Planktic Foraminifera (PF) shells are useful archives for studying the history of Earth's
55 climate and oceans, as their calcareous shells reflect the environmental conditions during their
56 formation (Berggren et al., 1995; Rosenthal, 2007; Schiebel & Hemleben, 2017; Kucera, 2007;
57 Katz et al., 2010; Gupta, 1999; Davis et al., 2020, and others). Various element/Ca measured
58 in PF tests have been closely linked to ambient seawater temperature (e.g., Mg/Ca; Rosenthal
59 et al., 2004), salinity (e.g., Na/Ca; Mezger et al., 2016; Gray et al., 2023), pH and the carbonate
60 system (e.g., B/Ca; Babila et al., 2014; Henehan et al., 2015; Haynes et al., 2019), productivity
61 (e.g., Ba/Ca; Fritz-Enders et al., 2022), and chemical weathering (e.g., Ti/Ca; Amaglio et al.,
62 2025, among others. In the past, the use of these proxies relied on bulk analysis of the entire
63 shell or multiple shells. However, in recent years there has been an increase in the use of high-
64 resolution analytical techniques, such as Laser Ablation (LA) ICP-MS and electron microprobe
65 analyses in paleoceanographic studies (Davis et al., 2020). The element/Ca measurements of



66 single specimens (Individual Foraminifer Analysis, IFA) revealed high variability between
67 individuals of the same population as well as significant intra-shell variability (i.e., inter
68 chamber variability, ICV) (Sadekov et al., 2008; Fehrenbacher et al., 2020; Hupp &
69 Fehrenbacher, 2024; Fischer et al., 2024; Davis et al., 2020, and references therein). The
70 associated changes in the geochemical signatures of PF shells are poorly understood and
71 despite the analytical advancements, there are still knowledge gaps in our understanding of
72 proxy systematics in single shell and single chamber of PF species although they are potentially
73 related to the observed shell and chamber element/Ca variability, the life cycles and
74 reproductive modes of many species, as they calcify their shell chambers one at a time. There
75 is also a lack of detailed description and understanding of proxy systematics in description of
76 the dynamics of small-sized species such as *T. clarkei*, which have been largely overlooked in
77 previous studies despite their significant contribution to the settling PF tests (export flux), as
78 observed in the northern Red Sea (Chernihovsky et al., 2018). Furthermore, specific marine
79 regions, such as in oligotrophic, subtropical basins, particularly in deep-water column
80 environments, are not well-established in terms of their spatial and temporal dynamics
81 (Schiebel & Hemleben, 2017).

82 1.2 Planktic Foraminifer population dynamics in The Gulf of Aqaba

83 The Gulf of Aqaba (GOA) is considered an open ocean proxy environment (Chase et al.,
84 2011). It is an oligotrophic basin where the main lithogenic flux is derived from dust. During
85 summer (April-September), a ~200 m deep thermocline separates nutrient-depleted surface
86 waters (~25°C) from the nutrient-rich deep layer (~21°C). In winter/spring (October-April),
87 the thermocline gradually erodes due to surface cooling (Figs. 1a and 1e; Meeder et al., 2012),
88 which can lead to the development of a deep mixed layer. Although the depth of the mixed
89 layer varies annually with climatic conditions, the long-term mean mixing depth is
90 approximately 300-400 m, and deep mixing can extend to the sea floor while it typically
91 reaches maximum depth by late March. The regional terrestrial climate is hyper-arid (mean
92 annual rainfall <30 mm) and the main sources for terrigenous material to the GOA are dust
93 storms originating from the Sahara and Arabian Deserts, as well as rare localized floods (Katz
94 et al., 2015; Chase et al., 2011; Ganor et al., 2001; Torfstein et al., 2017).



95
96 Figure 1: Time series of temperature (a), salinity (b), pH (c), Chlorophyll-a concentration (d),
97 and in situ density anomaly (e), measured in the Gulf of Aqaba between April 2014 and June
98 2015 by the National Monitoring Program (NMP, Shaked & Genin, 2016). Y-axis is depth (m);
99 A map of the Gulf of Aqaba (f); and (g) scanning electron micrographs of the three morpho-
100 species (exhibiting ablation holes in each chamber (labelled), from Levy et al., 2023).

101

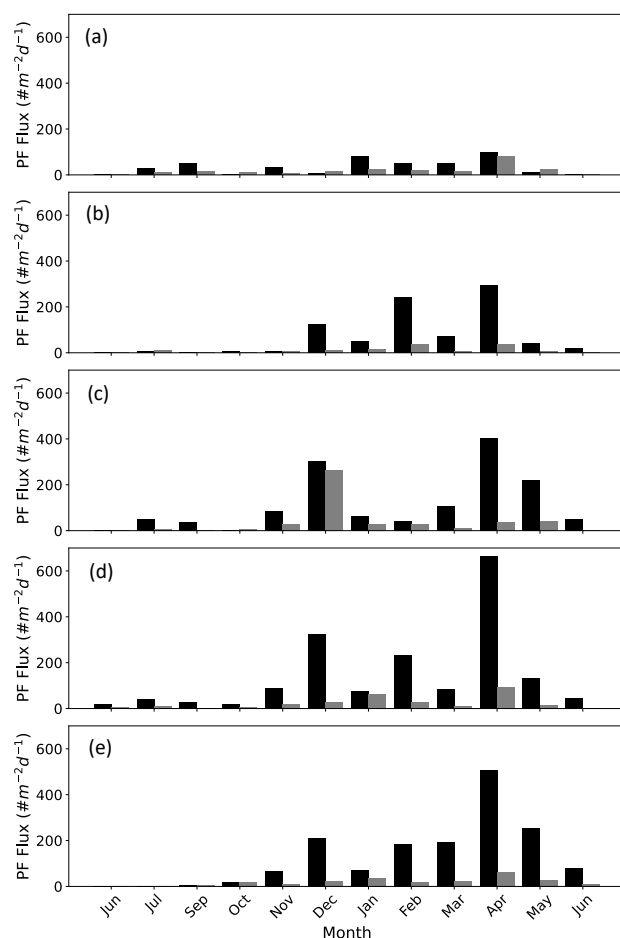
102 Planktic foraminifera fluxes in the GOA demonstrate strong seasonality, with low fluxes
103 during the summer months, gradually increasing during the autumn-winter, coeval with
104 decreasing sea-surface temperatures and deepening of the mixed layer in the GOA that drives
105 advection of nutrient-replete subsurface waters into the mixed layer. This in turn triggers an
106 increase in primary productivity, expressed by enhanced chlorophyll-a concentrations and high
107 PF fluxes (Chernihovsky et al., 2018, 2020).

108 Spinose species constitute the majority of the PF assemblage. The smaller size fraction,
109 63-125 µm, is 86% from the total flux and is dominated by *T. clarkei*. The 125-500 µm size-
110 fraction (~13 %) is dominated by the species *G. ruber albus*, while less than 1% of the shells
111 are in the range of 500-1000 µm, dominated by *O. universa* (Chernihovsky et al., 2018).

112 *Globigerinoides ruber albus* and *T. clarkei* inhabit different dwelling-depths and have
113 diverse life strategies. *Globigerinoides ruber albus* is a surface dweller and is photo-symbiont



bearing, while *T. clarkei* tends to dwell below the mixed layer depth and is barren of photo-symbionts (Rebotim et al., 2017; Schiebel & Hemleben, 2017; Levy et al., 2023). Furthermore, it has been suggested that *G. ruber albus* and *T. clarkei* do not share the same dietary preferences: *G. ruber albus* being more carnivorous than the detritivorous *T. clarkei* which may forage at the exported matter below the pycnocline (Schiebel & Hemleben, 2017). In the GOA, *T. clarkei* has two phenotypes: *T. clarkei* ‘big’, which all of its test chambers are fully recognizable and their surface is relatively smooth and *T. clarkei* ‘encrusted’ with a less smooth shell surface and is smaller than the ‘big’ type (Levy et al., 2023).



122

123 Figure 2: PF fluxes in the Gulf of Aqaba between June 2014 and June 2015 presented according
124 to the size fractions >63-125 μm (black bars) and >125-500 μm (grey bars) at the different
125 sediment trap depths a) 120 m, b) 220 m, c) 340 m, d) 450 m, and e) 570 m. Data from
126 Chernihovsky et al. (2018).



In this study, we investigate the range of element values, year-round trends and inter-chamber element/Ca variability in *G. ruber albus* and *T. clarkei* tests collected in sediment traps at various water column depths from the GOA. We assess whether the chambers record temporal-seasonal patterns, and the implications for using single chamber data for geochemical proxies (Mg/Ca, B/Ca, Na/Ca). Understanding inter-chamber variability sheds light on biomineralization processes and environmental factors that occur during different stages of the organism's life cycle. This in turn improves the calibration of element/Ca as proxies for reliable reconstruction of past oceanic and climatic conditions. Focusing on PF from the GOA provides critical insights into the use of foraminiferal element/Ca as proxies in a warm and hyper-saline oligotrophic environment.

2. Methodology

2.1. Sampling and oceanographic data

A bottom-tethered mooring has been deployed continuously since January 2014 near Station A, northern GOA (29° 28'95" N, 34° 56'22" E, ~605 m water depth) (Torfstein et al., 2020). Five KC Denmark cylinder sediment traps were mounted vertically and located at depths of 120 m, 220 m, 350 m, 450 m, and 570 m. The trap samples were collected at a monthly resolution. Furthermore, PF samples from the sediment interface were collected using a box core ('core top'). Further detailed description of the mooring, sampling, sample processing, and trapping efficiencies can be found in Chernihovsky et al. (2018) and Torfstein et al. (2020). Here, we report the findings derived from the PF tests collected between June 2014 and June 2015. Water column physical and chemical parameters are routinely collected at Station A by the Israel National Monitoring Program (NMP, Shaked & Genin, 2016). This includes sea surface and water column temperature (°C), salinity, oxygen concentration (μmol/l), alkalinity (meq/kg), pH, and chlorophyll-a concentration (μg/l). The mixed layer depth (MLD) is defined as the water depth where the density anomaly (σ_0) is equal to, or above, the water density of the surface water column plus a density threshold of 0.125 kg/m³ (Sprintall & Tomczak, 1992).

2.2. Species classification and preparation for LA-ICP-MS



We examined the shell chemical properties of two flux dominating PF species *T. clarkei* and *G. ruber albus* (i.e., sensu stricto, white). For *T. clarkei* we examined two morphotypes: ‘big’ and ‘encrusted’. Identification and nomenclature of the PF taxa followed Schiebel & Hemleben (2017), Morard et al. (2019), and Brummer & Kucera (2022). Three individuals were picked from each sediment trap depth during each month between June 2014 and June 2015. Preliminary preparation and cleaning steps are detailed by Chernihovsky et al. (2018). Reductive and oxidative cleaning had been avoided to retain original signals related to the different encrustation processes and preserve all calcite layers added to the shell during ontogeny (Schiebel & Hemleben, 2017; Jochum et al., 2019). Specifically, the shell *T. clarkei* is prone to loss of material during reductive and oxidative treatment as it has very thin shells with a width ranging 1.9-3.6 μm (Levy et al., 2023). Single chamber measurements were performed to assess inter chamber variability (ICV), on individual shells (individual foraminifer analysis; IFA) using Laser Ablation Inductively Coupled Plasma Mass Spectrometry (LA-ICP-MS) on 156 specimens in total. Samples were glued to glass slides using a methyl-hydroxy-propyl-cellulose (MHPC 1:100), positioned with the umbilical side up.

2.3. LA-ICP-MS and data processing

Analyses of the calcium-normalized elements for B, Na, Mg, Al, Ti, Mn, Fe, Co, Sr, Ba, Nd, Pb, Th, and U were conducted using a 200 nm wavelength NWR femtosecond (fs) LASER system from ESI, combined with a sector-field Thermo Element-2 ICP mass spectrometer (Jochum et al., 2014). Measurements were performed using a 15 Hz pulse repetition rate (PRR), at low fluence (0.1–0.6 J/cm²), and 18 seconds dwelling time. A 30 μm diameter spot size was selected, as it is the maximum diameter for analysis fitting in a single chamber of the small *T. clarkei*. The microanalytical synthetic reference material MACS-3 for carbonate, NIST-612, and NIST-610 were used for calibration. NIST-612 was used for the tuning of the ICP-MS (Jochum et al., 2019).

The measurement precision (1 relative standard deviation in percent; 1 RSD) yield uncertainties for references materials between ~ 5-17 % for the calcium-normalized elements (Supplementary table 1). Single spot measurements were made on each chamber of the individual shells. Chambers are labelled F0 (final chamber), F-1 (final minus one), F-2, and so on, for the penultimate, antepenultimate, and further chambers, respectively. We calculated averages and standard deviations of element/Ca of single individuals (calculated from all single



190 chamber element /Ca in one shell) and relative standard errors of element/Ca of pooled
191 measurements for a specific morphotype.

192 3. Results:

193

194 3.1. Depth-averaged values of element/Ca measured in *G. ruber albus* and *T. clarkei*
195 shells using LA-ICP-MS

196

197 Generally, the means of Mg/Ca, Sr/Ca, B/Ca, Na/Ca and Ba/Ca in *G. ruber albus* indicate that
198 the composition of tests, from most water depths is similar to that of core-top samples (Figs.
199 3a-3d, 3j). In contrast, Al/Ca, Ti/Ca, Mn/Ca, Fe/Ca, Nd/Ca, Th/Ca, and U/Ca (Figs. 3e-3i, 3k,
200 3m, 3n) in the tests from sediment interface were higher than in the water column, and lower
201 in case of Co/Ca and Pb/Ca (Figs. 3i, 3l).

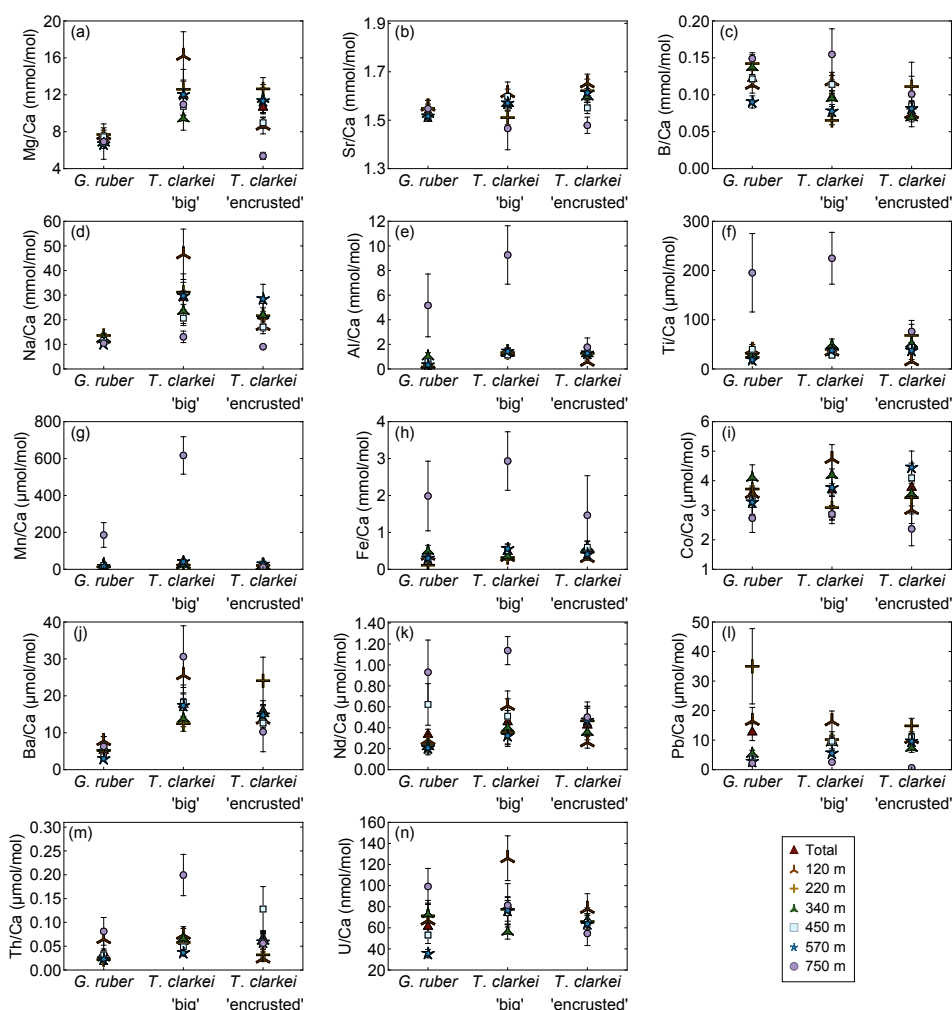


Figure 3: Pooled mean values of the calcium-normalized element ratios of *G. ruber albus*, *T. clarkei* 'big' and *T. clarkei* 'encrusted' shells, derived from sediment traps located at different water depths (120 m to 570 m) and a core top sample (750 m) from the Gulf of Aqaba. Error bars represent 1 sigma relative standard error (SD/\sqrt{n}).

Furthermore, *T. clarkei* tends to demonstrate higher values and higher variability compared to *G. ruber albus*. Compared to the core-top samples, *T. clarkei* from the water column also exhibit relative enrichment in Al/Ca, Ti/Ca, Mn/Ca, Fe/Ca, Nd/Ca, B/Ca, and Th/Ca (*T. clarkei* 'big'), and depletion in Co/Ca, Pb/Ca, Sr/Ca, and Mg/Ca (*T. clarkei* 'encrusted') (Fig. 3).

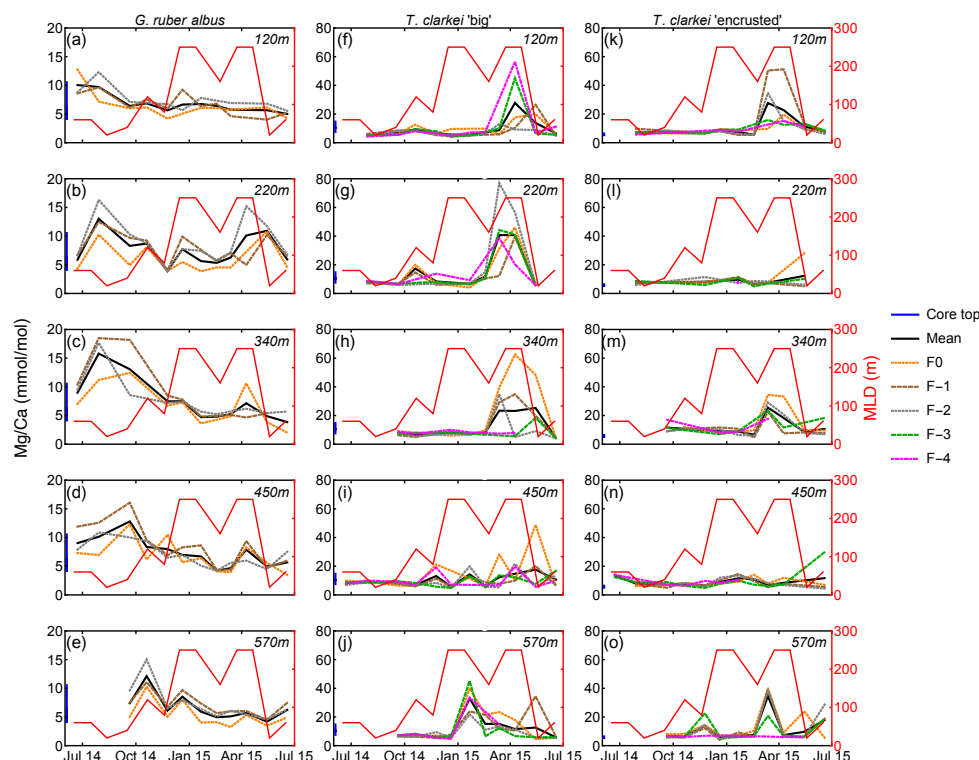
3.2. Shell-bound element/Ca time series trends in *G. ruber albus* and *T. clarkei* shells



214

215 Pooled mean values of Mg/Ca in *G. ruber albus* taken from all water column depths in the
216 GOA reflect MLD temperatures (Fig. 10). Single chamber Mg/Ca over water column depths
217 in *G. ruber albus* range between 2.01 mmol/mol (340 m; June 2015) and 18.49 mmol/mol (340
218 m; July 2014), with lower/higher values during winter/summer months, respectively (Figs. 4a-
219 4e). A unique observation is an increase in Mg/Ca seen during spring (March-April), i.e.,
220 months with maximum surface water column mixing, at some water depths (220 m, 340 m,
221 450 m; Figs. 4b-4d). Accompanied with the Mg/Ca increase is a clear increase in ICV as
222 evident by the divergence of chamber values. Generally, it appears that Mg/Ca is lower in F0
223 chambers (orange dotted line) compared to preceding chambers. Mg/Ca in *T. clarkei* ‘big’
224 range between 4.00 mmol/mol (340 m; June 2015) and 77.02 mmol/mol (220 m; March 2015)
225 and between 4.06 mmol/mol (570 m; December 2014) and 51.22 mmol/mol (120 m; April
226 2015) in *T. clarkei* ‘encrusted’, respectively.

227



228

229 Figure 4: Time series of Mg/Ca values measured from the shells of *G. ruber albus* (a-e), *T.*
230 *clarkei* ‘big’ (f-j) and *T. clarkei* ‘encrusted’ (k-o), derived from sediment traps located at



different water depths (120–570 m). Mg/Ca of core top are marked by a blue bar along the left y-axes.

Sr/Ca in *G. ruber albus* range between 1.25 mmol/mol (570 m; January 2015) and 2.27 mmol/mol (340 m; November 2014) (Figs. 5a–5e). Single chamber Sr/Ca in *T. clarkei* ‘big’ range between 0.94 mmol/mol (340 m; January 2015) and 2.76 mmol/mol (220 m; April 2015) and for *T. clarkei* ‘encrusted’ between 0.54 mmol/mol (340 m; April 2015) and 2.92 mmol/mol (570 m; June 2015), respectively (Figs. 5f–5j, and 5k–5o). *Turborotalita clarkei* ‘big’ and *T. clarkei* ‘encrusted’ display more ICV than *G. ruber albus*, with peaking Sr/Ca in numerous chambers around April 2015 (Figs. 5f–5o). During the spring months of 2015, Sr/Ca values range between 1.45–2.04 mmol/mol in *G. ruber albus*, 1.32–2.76 mmol/mol in *T. clarkei* ‘big’ and 0.54–2.27 mmol/mol in *T. clarkei* ‘encrusted’, respectively (Fig. 5; Fig. S1).

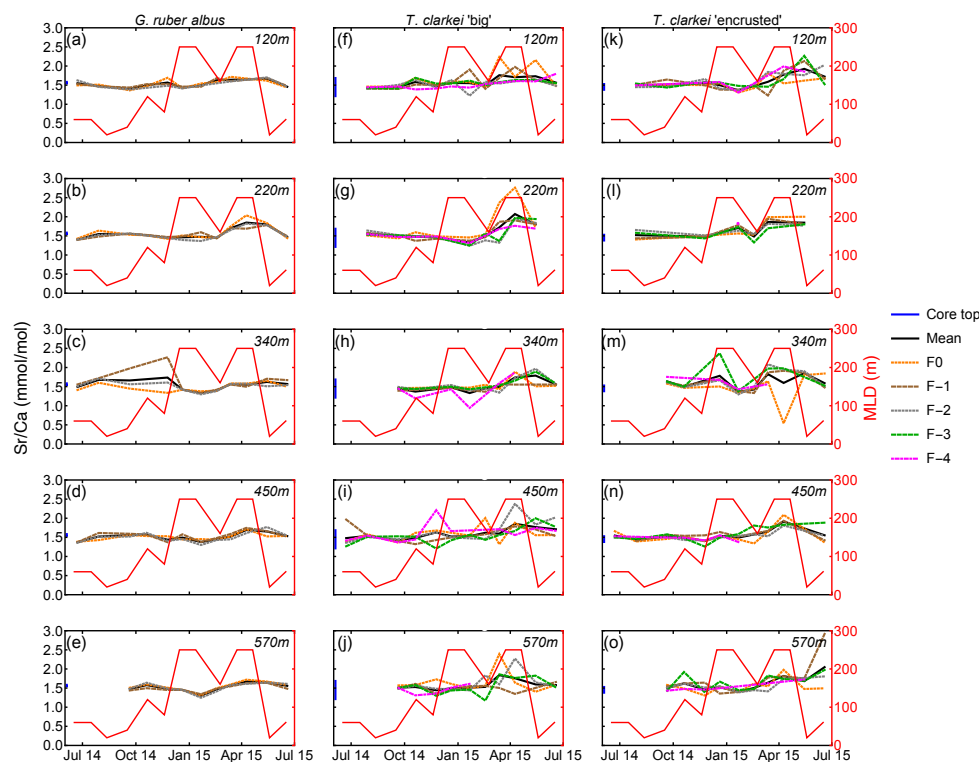
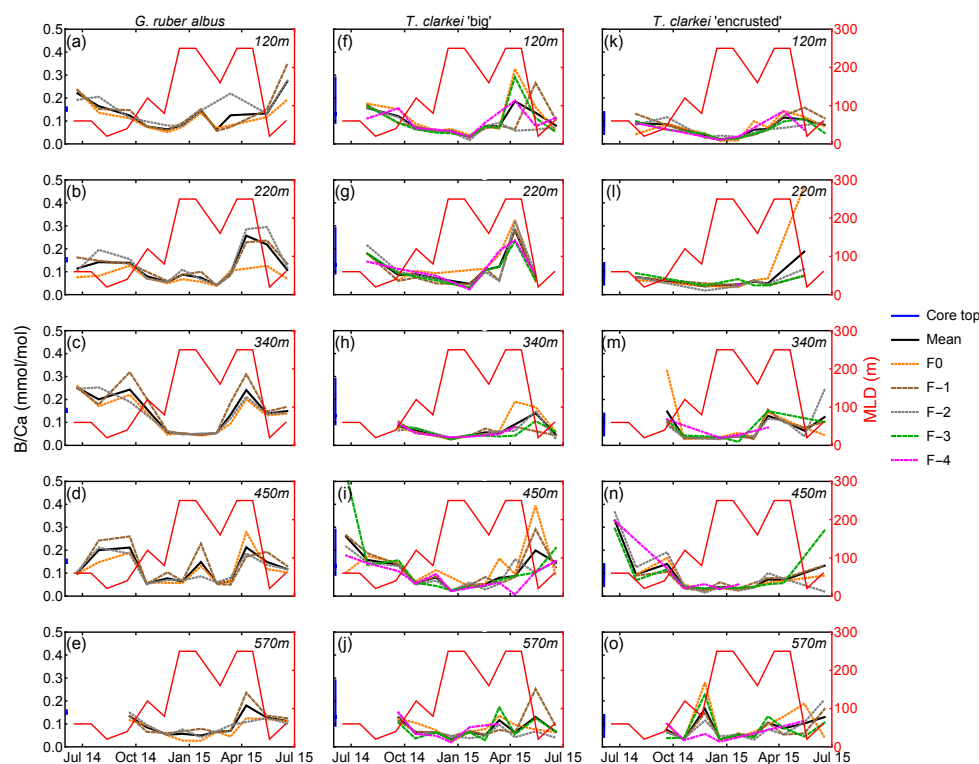


Figure 5: Time series of Sr/Ca values measured from the shells of *G. ruber albus* (a–e), *T. clarkei* ‘big’ (f–j) and *T. clarkei* ‘encrusted’ (k–o), derived from sediment traps located at different water depths (120 m – 570 m).



248

249 B/Ca values range between 0.03 mmol/mol (570 m; January 2015) to 0.35 mmol/mol (120 m;
250 June 2015) in *G. ruber albus*, with higher values during summer and spring and lower values
251 during the winter (Figs. 6a to 6e). B/Ca measured in the final chamber, F0, are systematically
252 lower compared to F-1 and F-2 values. Unlike most other element ratios, B/Ca values in both
253 phenotypes of *T. clarkei* are similar to the range measured in *G. ruber albus*. In both *T. clarkei*
254 phenotypes, lower B/Ca values were measured during the winter months, most prominently in
255 January. The B/Ca values of *T. clarkei* ‘big’ range between 0.01 mmol/mol to 0.53 mmol/mol
256 with some higher values during spring (Figs. 6f to 6j). B/Ca values in *T. clarkei* ‘encrusted’
257 range between 0.01 mmol/mol to 0.47 mmol/mol. Generally, B/Ca ICV is higher in *T. clarkei*
258 than *G. ruber albus*, especially during spring.



259

260 Figure 6: Time series of B/Ca values measured from the shells of *G. ruber albus* (a-e), *T. clarkei*
261 ‘big’ (f-j) and *T. clarkei* ‘encrusted’ (k-o), derived from sediment traps located at different traps
262 from 120 m to 570 m water depths.

263

264



Na/Ca in *G. ruber albus* ranges between 6.60 mmol/mol (220 m; June 2014) to 64.14 mmol/mol (220 m; April 2015) with a median value of 10.43 mmol/mol (Fig. 7; Fig. S1). Na/Ca in *T. clarkei* ‘big’ ranges from 6.23 mmol/mol (570 m; September 2014) to 426.54 mmol/mol (220 m; March 2015) with a median value of 12.33 mmol/mol. Na/Ca in *T. clarkei* ‘encrusted’ ranges between 5.43 mmol/mol (570 m; September 2014) to 176.91 mmol/mol (570 m; March 2015) with a median value of 12.41 mmol/mol. *Globigerinoides ruber albus* has a low ICV during spring, while *T. clarkei* ‘big’ and ‘encrusted’ phenotypes display higher ICV during the same time interval. All morphotypes include significant excursions in Na/Ca with high values in *G. ruber albus* during January and April at 220m (Fig. 7b), and high Na/Ca in both *T. clarkei* phenotypes at multiple depths and seasons (Figs. 7f-7j and 7k-7o). In particular, *T. clarkei* phenotypes show significant Na/Ca excursions during March-April and ICV (Figs. 7f-7o).

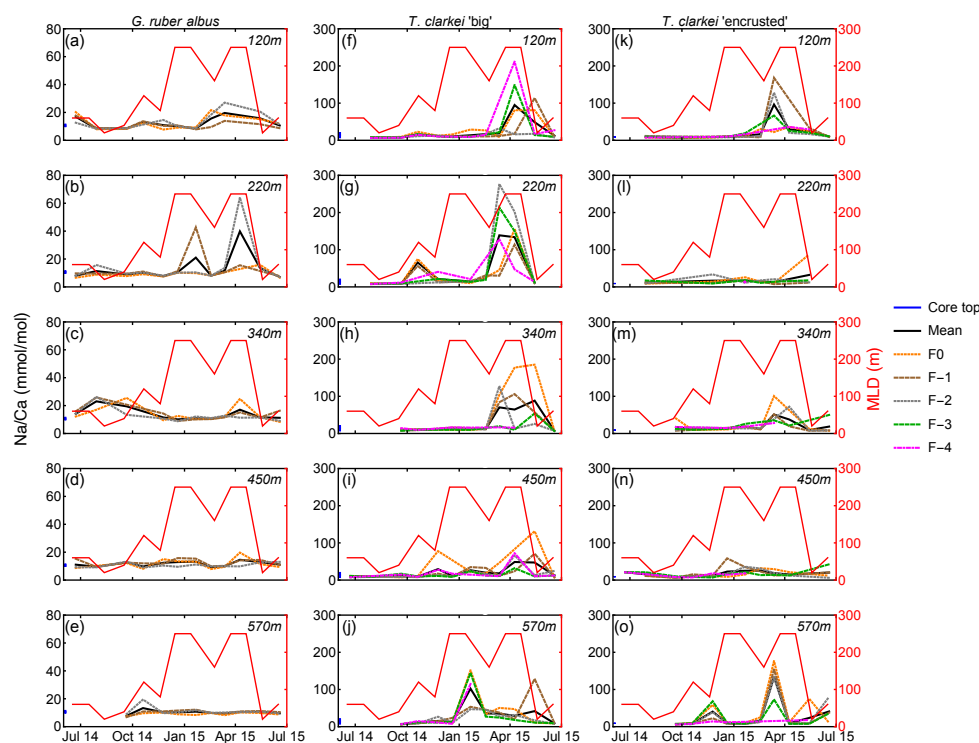


Figure 7: Time series of Na/Ca values measured from the shells of *G. ruber albus* (a-e), *T. clarkei* ‘big’ (f-j) and *T. clarkei* ‘encrusted’ (k-o), derived from sediment traps located at different water depths (120 m – 570 m).

280

Ba/Ca in *G. ruber albus* ranges from 0.73 $\mu\text{mol/mol}$ (120 m; November 2014) to 36.81 $\mu\text{mol/mol}$ (340 m; June 2015). Ba/Ca in *T. clarkei* ‘big’ ranges from 0.39 $\mu\text{mol/mol}$ (120 m;



June 2015) to 246.54 $\mu\text{mol/mol}$ (450 m; March 2015). Ba/Ca in *T. clarkei* ‘encrusted’ ranges from 0 $\mu\text{mol/mol}$ (April 2015) to 171.41 $\mu\text{mol/mol}$ (340 m; March 2015) (Fig. 8; Fig. S1). The three morphotypes display varied ICV, although *T. clarkei* shows more prominent ICV during spring months (Figs. 8f-8o) than *G. ruber albus* (Figs. 8a-8e).

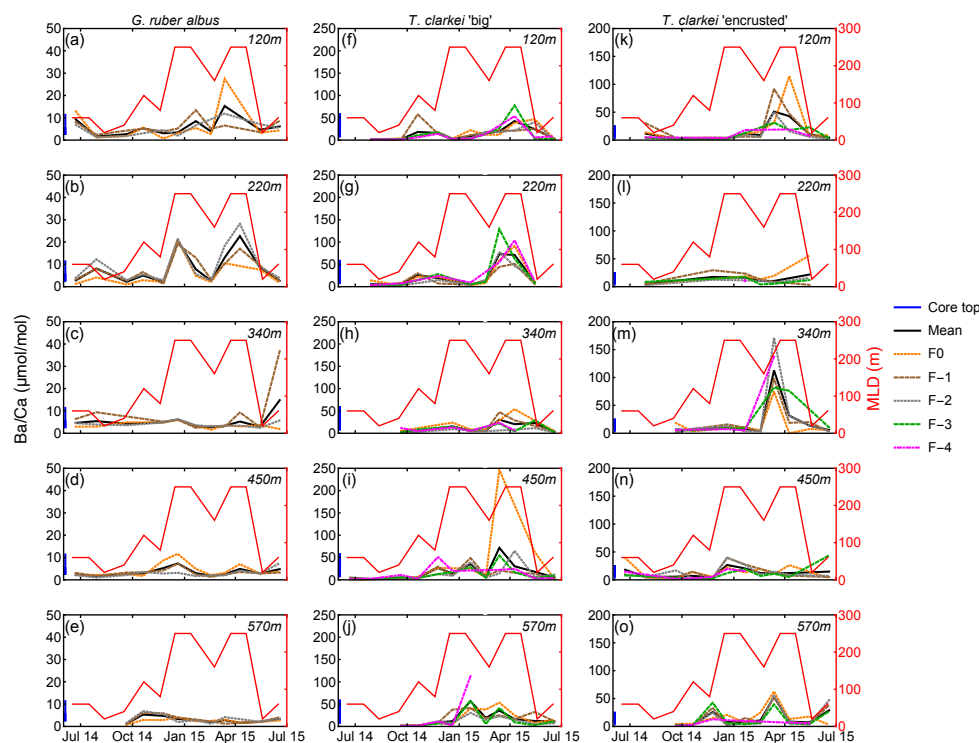


Figure 8: Time series of Ba/Ca values measured from the shells of *G. ruber albus* (a-e), *T. clarkei* ‘big’ (f-j) and *T. clarkei* ‘encrusted’ (k-o), derived from sediment traps located at different water depths (120 m – 570 m).

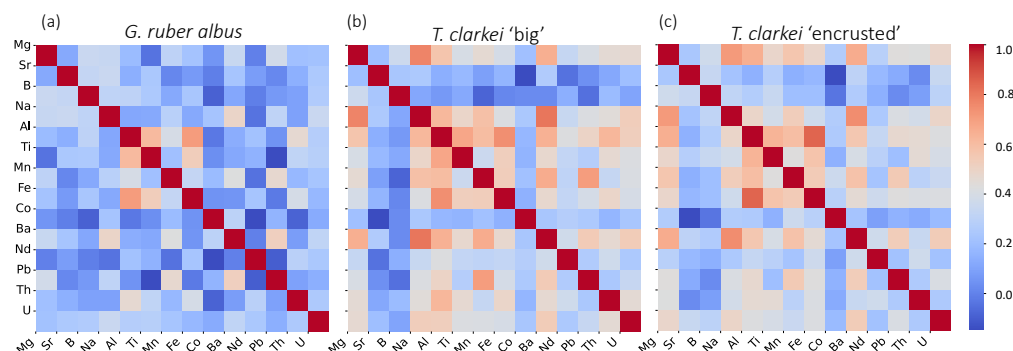
3.3. Relationships between element/Ca of the different PF species in the GOA

A Spearman correlation matrix was applied to assess the numerical relationships of the element/Ca in the three analyzed PF phenotypes (Fig. 9; Tab. S2). The *T. clarkei* types exhibit similar pattern of relationships, with minor differences mainly in correlation strength (Fig. 9a, 9b). In general, *T. clarkei* shows more significant relationships than *G. ruber albus*, while, *G. ruber albus*, display different relationships to those of the two *T. clarkei* types. In *T. clarkei*, Mg/Ca displays relatively strong relationships with Na/Ca, Ba/Ca, and Al/Ca (Fig. 9b, 9c). Sr/Ca, B/Ca, Co/Ca and Nd/Ca do not display significant relationships to other elements in *G. ruber albus* as well as in *T. clarkei* ‘big’ and *T. clarkei* ‘encrusted’.



301

302



303

304 Figure 9: Spearman correlation Matrix of the different trace element Ca normalized abundances

305 in *G. ruber albus* (a), *T. clarkei* “big” (b) and, *T. clarkei* “encrusted” (c).

306

307 For both *T. clarkei* ‘big’ and *T. clarkei* ‘encrusted’, Na/Ca significantly correlates with
 308 Al/Ca, Mn/Ca, and Ba/Ca, the later showing the strongest relationships in *T. clarkei* ‘big’ ($r =$
 309 0.82, Fig. 9b; Tab. S2). Relationships between Al/Ca, Ti/Ca, Mn/Ca, Fe/Ca, Ba/Ca and Th/Ca
 310 are generally stronger in *T. clarkei* ‘big’ than in *T. clarkei* ‘encrusted’, except for Al/Ca and
 311 Fe/Ca, which are stronger related in *T. clarkei* ‘encrusted’ ($r = 0.85$; Tab. S2) than in *T. clarkei*
 312 ‘big’ ($r = 0.74$; Tab. S2). Unlike *G. ruber albus*, the U/Ca in *T. clarkei* exhibit relatively strong
 313 relationships with Ba/Ca, Na/Ca and Al/Ca (in *T. clarkei* ‘big’) and Mg/Ca (in *T. clarkei*
 314 ‘encrusted’, Fig. 9c) while in *G. ruber albus*, U/Ca is poorly related to the other elements (Fig.
 315 9a).

316

317 4. Interpretation

318 4.1 Inter chamber variability (ICV)

319 Shell-bound element/Ca display varying trends across different chambers depending on the
 320 specific element ratios, and varying over water depth and time (Figs. 4-8). Typically, most PF
 321 reproduction-cycles span about a month with individual chambers forming within several hours
 322 (Bé et al., 1977), while the time interval between chamber formation can range from hours to
 323 weeks (Schiebel & Hemleben, 2017, and references therein). Setting aside the March-April
 324 time-interval where PF shells show exceptionally high ICV, *G. ruber albus* generally exhibits
 325 lower values (e.g., Mg/Ca, B/Ca), and less ICV compared to *T. clarkei* ‘big’ and ‘encrusted’.
 326 The residence of *G. ruber albus* in the relatively homogenous and narrow living environment



327 in the surface mixed layer (Schiebel & Hemleben, 2017; Thirumalai et al., 2014; and others),
328 could explain relatively lower ICV. In contrast, *T. clarkei* dwell in the dynamic region
329 near/under the thermocline (Schiebel & Hemleben, 2017; Levy et al., 2023) over a wider
330 dwelling depth horizon, and may experience more heterogeneous environmental conditions
331 which may result in higher ICV.

332 The secondary crust observed on *T. clarkei* 'encrusted' morphotypes, which covers all
333 chambers of the tests analysed here, does not significantly alter element/Ca when compared to
334 *T. clarkei* 'big', unlike the crust of *Neoglobobadrina dutertrei* (Jonkers et al., 2012). This
335 suggests that the secondary calcite layer in *T. clarkei* 'encrusted' does not play a major role in
336 element incorporation or ICV and is affected by the same mechanisms which control the
337 formation of the ontogenetic calcite, and thus would facilitate application of our finding to the
338 interpretation of fossil *T. clarkei* 'encrusted' in paleoceanography and paleoclimate
339 reconstructions.

340 The ultimate chamber (F0) presents different systematics compared to the preceding
341 chambers in both *T. clarkei* and *G. ruber albus* (Fig. S11). In *T. clarkei* (both 'big' and
342 'encrusted'), the F0 typically exhibits higher values of B/Ca, Na/Ca, Mg/Ca, and Al/Ca
343 compared to the previous chambers. In contrast, *G. ruber albus* displays relatively lower values
344 in F0 for the same ratios highlighting species-specific differences in chamber formation (Fig.
345 S11). Interestingly, Sr/Ca does not follow the same pattern. In *T. clarkei* 'big' the Sr/Ca
346 distribution mirrors the trends of other elements, while F0 in *G. ruber albus* and *T. clarkei*
347 'encrusted' shows an even distribution of Sr/Ca, likely reflecting the relatively constant Sr/Ca
348 values in the water column during the lifespan of a single test. These observations in *G. ruber*
349 *albus* are consistent with previous studies that measured Mg/Ca in individual chambers (Bolton
350 et al., 2011; Davis et al., 2020; Fischer et al., 2024). The contrasting systematics of F0 leading
351 to elevated ICV in the ultimate chamber compared to the previous chambers was previously
352 suggested to be associated with a chamber wall that is not fully calcified (Schiebel &
353 Hemleben, 2017; Bolton et al., 2011; Fischer et al., 2024). Differences in F0 systematics
354 between *T. clarkei* and *G. ruber albus* could be driven by species-specific calcification
355 processes, though further research is needed to clarify this issue. Additionally, it is important
356 to consider potential biases in small chambers such as F-4 in *T. clarkei* morpho-species, where
357 methodological challenges (e.g., laser spots hitting sutures) may skew element/Ca
358 measurements. Consequently, we conclude that the exclusion of F0 and F-4 will enhance the
359 reliability of reconstructions of the marine environment in studies of downcore records.

360



4.2 Relationships of element ratios of the three PF morphotypes

The contrasting results of the correlation matrixes of the three morphospecies, suggests species-specific mechanisms while calcifying their shells. The Mg/Ca in *T. clarkei* which strongly correlates with Na/Ca, Ba/Ca, and Al/Ca (Fig. 9c), suggests more than one environmental process affects Mg/Ca in the tests as the other element/Ca are considered proxies to different environmental characteristics such as salinity, productivity, and terrigenous input (Chang et al., 2015; Mesa-Fernández et al., 2022; Beasley, et al., 2021). Similar to *G. ruber albus*, in the *T. clarkei* types Sr/Ca, B/Ca, Co/Ca and Nd/Ca do not display statistically significant relationships to other elements making them suitable proxies for distinct and independent environmental properties.

In *G. ruber albus*, Mg/Ca, Sr/Ca and B/Ca show no significant relationships with other element ratios, indicating that independent processes likely govern their proxy systematics (Fig. 9c). Similarly, Co/Ca, Nd/Ca and U/Ca also do not correlate with other element/Ca. While Na/Ca and Ba/Ca exhibit some degree of correlation, as do Mn/Ca and Pb/Ca, the lithophilic elements, Al/Ca, Ti/Ca, which are considered proxies for terrigenous dust input (Chang et al., 2015; Mesa-Fernández et al., 2022; Beasley, et al., 2021), as well as, Fe/Ca, and Th/Ca, all show a relative strong correlation. Their correlation implies they can be used together for reconstructing terrigenous input to the water column. Among the lithophilic elements, Th/Ca display a relatively weaker relationship, suggesting a potential effect of additional processes such as scavenging (Anderson et al., 1983; Francois et al., 2004; Costa et al., 2020).

4.3 Mg/Ca as a proxy for sea surface temperature

Shell-bound Mg/Ca of calcareous foraminifera have been extensively utilized as a paleothermometer (e.g., Nürnberg et al., 1996; Sadekov et al., 2009). Many of these Mg-temperature calibrations rely on whole-test or pooled-mean Mg/Ca values to reconstruct past sea surface temperatures (Spero et al., 2003; Ganssen et al., 2010; and others). Several studies have measured intra-test and inter-test Mg/Ca in an effort to produce Mg-temperature calibrations using single chamber measurements of *G. ruber* (Sadekov et al., 2008; Bolton et al., 2011; Davis et al., 2020; Levy et al., 2023; Fischer et al., 2024). Previous work on sediment trap-derived specimens of *T. clarkei* and *G. ruber albus* from the GOA indicated that *T. clarkei* is not suitable for temperature reconstructions, due to its presumed deep dwelling-depth below the thermocline together with its high sensitivity to water column mixing events. However, while *G. ruber albus* shows exceptionally high pooled mean Mg/Ca values in the GOA in comparison to other ocean regions, it also exhibits seasonal variations that indicate effective



applicability as a paleothermometer (Levy et al., 2023). Due to the high seawater salinity of the GOA, a local calibration curve was proposed (Eq. 1; Levy et al., 2023).

$$\frac{\text{Mg}}{\text{Ca}} = 0.39(\pm 0.30) \cdot e^{0.12(\pm 0.03)T} \quad (1)$$

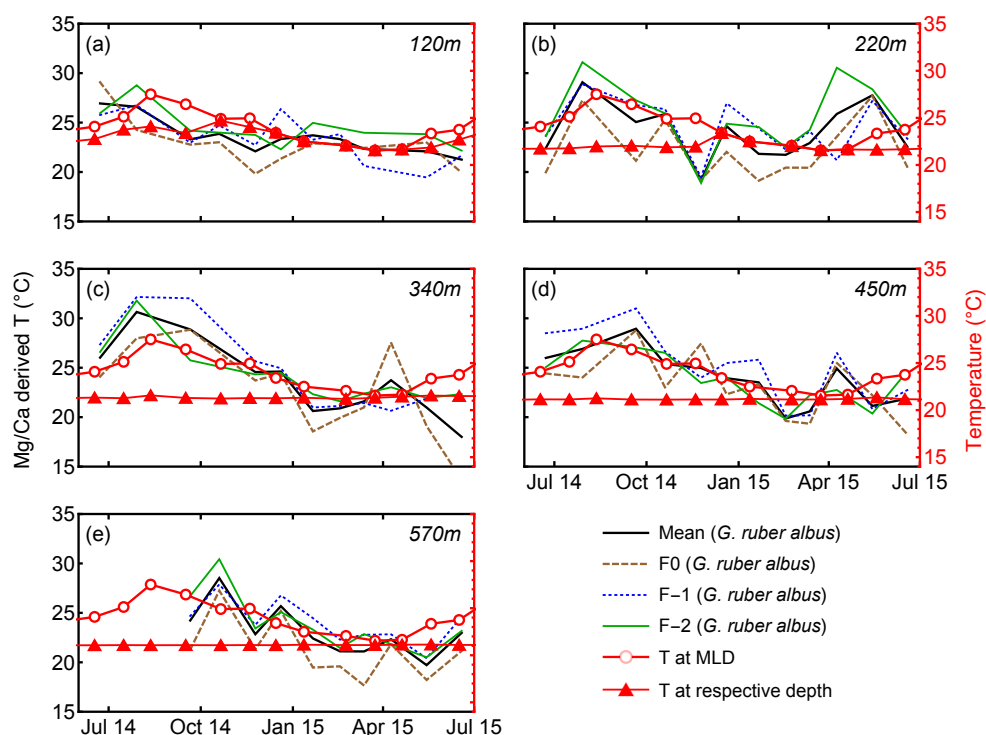


Figure 10: *G. ruber albus* Mg/Ca-derived temperatures versus measured temperatures (red). The calculated temperatures were derived from Eq. 1 for individual chambers. See also Levy et al. (2023).

Inter-chamber variability (ICV) has been shown to affect the local Mg/Ca temperature calibration (Eq. 1) of *G. ruber albus* (Levy et al., 2023; Fig. 10). Generally, Mg/Ca-derived temperatures from chambers F-1 and F-2 correspond closely with mixed layer depth (MLD) temperatures. However, beneath the photic zone, Mg/Ca of all three chambers F0, F-1, and F-2 of the *G. ruber albus* specimens exhibit poor fits with measured temperatures (Fig. 10). Given that *G. ruber albus* calcifies its shell in the photic zone (Schiebel and Hemleben, 2017), these findings support the use of Mg/Ca as a paleothermometer (Nürnberg et al., 1996). The Mg/Ca-



412 derived temperatures from chamber F0 show lower Mg/Ca temperatures of the MLD than
413 chambers F-1 and F-2 (Fig. 10). Although Mg/Ca data from chambers F-1 and F-2 appear
414 suitable for reconstructing temperatures and demonstrate agreement with MLD temperature
415 trends, the high ICV in *G. ruber albus* is evidently too great to accurately reflect ambient
416 temperatures using this calibration. Therefore, and based on these new observations, we
417 suggest that optimal Mg/Ca-temperature calibration (Eq. 1) should be based on the pooled
418 mean of the F-1 and F-2 chambers at all depths.

419

420 4.2 B/Ca as a proxy for pH

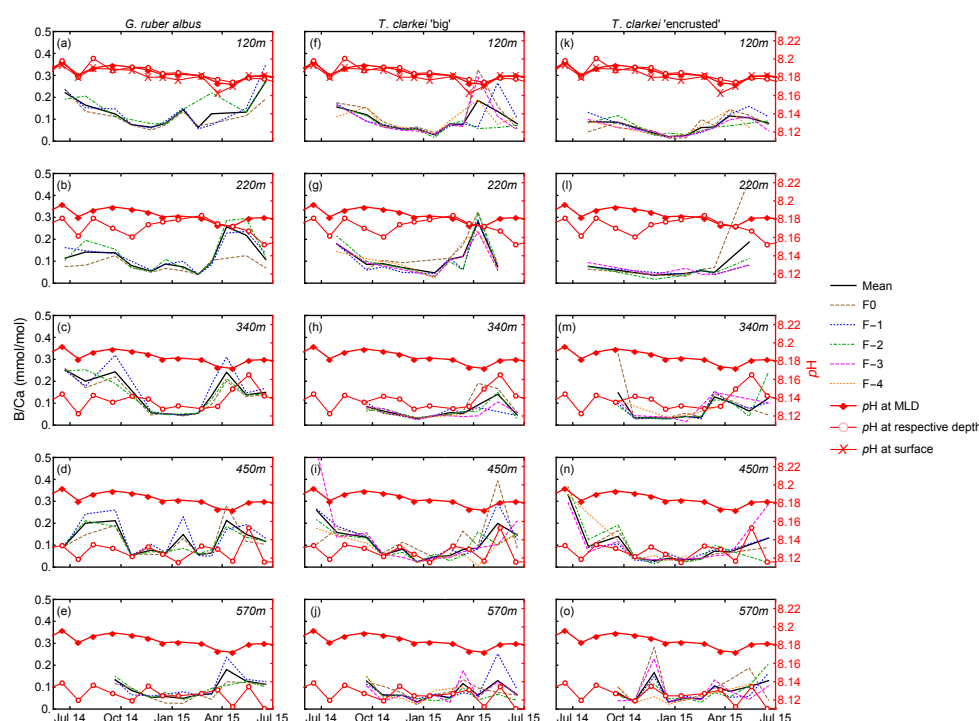
421 B/Ca in some PF species has been suggested to be a proxy for pH (Yu et al., 2007; Allen et al.,
422 2011). Comparing chamber B/Ca of both *G. ruber albus* and *T. clarkei* (both ‘big’ and
423 ‘encrusted’) alongside pH at various water column depths in the GOA reveals contrasting
424 results. While B/Ca in *G. ruber albus* exhibits seasonality (Fig. 6), with lower values during
425 winter months, it does not appear to be consistent with the pH of respective water depth nor
426 the MLD (Fig. 11). This inconsistency suggests that B/Ca in *G. ruber albus* from the GOA is
427 not a reliable recorder of ambient water pH. Similarly, Henehan et al. (2015) and Naik & Naidu
428 (2014) reported that B/Ca of open ocean core-top samples and down-core sediment samples do
429 not display a pH relationship.

430 Alternatively, B/Ca in *G. ruber albus* may be sensitive to salinity and micro-environments
431 produced by PF symbionts with pH levels which are distinct from the ambient water column.
432 Culture experiments have shown that B/Ca is affected by salinity and increases with increasing
433 salinity (Allen et al., 2012). However, only small salinity changes occur in the GOA (Fig. 1),
434 which argue against a strong B/Ca-salinity relationship that would result in a B/Ca seasonal
435 trends. It was suggested that photo-symbionts such as dinoflagellates in *G. ruber albus* create
436 micro-environments with pH levels, which are distinct from ambient seawater, to accommodate
437 for their photosynthetic activity, and indicate that B/Ca is more affected by pH in those micro-
438 environments than the water column pH (Hönisch et al., 2021; Babila et al., 2014). An
439 additional observation for the *G. ruber albus* B/Ca values is that they are relatively high in
440 comparison to values from other studies. The relatively high salinity in the GOA (~41),
441 combined with the photosymbiont activity in *G. ruber albus* may explain the elevated B/Ca
442 values (Henehan et al., 2015; Hönisch et al., 2021; Babila et al., 2014).

443 In contrast to *G. ruber albus*, B/Ca in the photosymbiont barren *T. clarkei* may indeed record
444 the changes in pH (Fig. 11) of seawater at its ambient dwelling depth, possibly shifting between
445 the deeper water column depth horizons where pH changes are evident. Indeed, based on the



446 fluxes of *T. clarkei* (Chernihovsky et al., 2018; Fig. 2), the B/Ca of *T. clarkei* in the sediment
447 record likely represent the *pH* beneath the thermocline and within the deep-water column
448 horizons for specimens that lived from early winter through spring. In particular, *pH* at 340 m
449 appears to correlate with the B/Ca trends of *T. clarkei* types. For B/Ca-*pH* calibrations utilizing
450 the pooled mean of data from the chambers F-1, F-2, and F-3 is recommended, while excluding
451 the F0 and F-4 chambers where more ICV is apparent (Fig. 11).



452 Figure 11: Single chamber B/Ca and in situ *pH* measured at MLD depth (empty red circles)
453 and 120 m water depth for *G. ruber albus*, *T. clarkei* 'big' and *T. clarkei* 'encrusted'.
454
455

456 4.3 Na/Ca as a proxy for salinity and Ba/Ca as an indicator for productivity

457 Cultured individuals and samples from the surface Caribbean and the Gulf of Guinea of live *T.*
458 *sacculifer* indicate that Na/Ca can be used as a proxy for salinity, without temperature
459 dependence, however, a species-specific calibration might be required (Bertlich et al., 2018).
460 Despite the high variability of PF Na/Ca values in the GOA during water column mixing (Fig.
461 7), salinity remains high and relatively constant, ranging between 40.4-40.7. Consequently, a
462 local Na/Ca-salinity calibration shows no significant relationship for any of the three PF
463 morphotypes.



Na/Ca values in PF from the GOA are notably higher compared to other regions. Gray *et al.* (2023) explored the relationship between Na/Ca and salinity in *G. ruber albus* collected from sediment traps, plankton tows, culture samples, and core top samples, contributing to the ongoing discussions regarding the reliability of Na/Ca as a proxy for salinity in both planktic and benthic foraminifera (Allen *et al.*, 2016; Geerken *et al.*, 2018; Mezger *et al.*, 2016, 2018; Gray *et al.*, 2023, and references therein). They concluded that the measurement method (i.e., ‘solution’ ICP-MS vs. LA-ICP-MS) influences the values of Na/Ca and in turn the relationship with salinity, i.e., weak in solution-based compared to significant in laser ablation-based, at salinity over 36.

Comparing Na/Ca of *G. ruber albus* from the shallowest sediment trap (120 m) in the GOA with the Na/Ca of *G. ruber albus* plankton tows-samples from the GOA deployed and collected in January 2010 and October 2013 (Gray *et al.*, 2023), both measured using LA-ICP-MS, generally reveals similar results, excluding the high-value excursions observed in some single chamber measurements (Fig. 7). *Turborotalita clarkei* in the GOA exhibits elevated Na/Ca values in both ‘big’ and ‘encrusted’ compared to *G. ruber albus*. Unlike *G. ruber albus*, there is relatively higher variability between water depths as well as significantly higher values in March, April, and May associated with water column mixing (Fig. 7). During these mixing events, nutrient-rich, high salinity (~40.7) water ascend upward. Therefore, the Na/Ca of *T. clarkei* may serve as a proxy for water column stability, i.e., stratification vs. mixing.

The Ba/Ca in the three morpho-species show a relatively strong correlation with Na/Ca (0.74 and 0.82 in *T. clarkei* ‘big’ and ‘encrusted’ respectively, and 0.54 in *G. ruber albus*, the second highest ratio and exceeded only by the 0.57 of Pb/Ca). Ba/Ca is presumably unaffected by temperature, salinity, and pH (Hönisch *et al.*, 2011). In non-spinose species, Ba/Ca typically shows positive relationships with productivity and potentially can be used as an indicator of river run-off (Fritz-Endres *et al.*, 2022; Hönisch *et al.*, 2011; Weldeab *et al.*, 2014). Although floods in the catchment area of the GOA are brief and occur only few times each year (Katz *et al.*, 2015), significant Ba/Ca perturbations during water column mixing may reflect nutrient-rich water admixing to the surface water (Fig. 8).

5. Discussion:

5.1 Temporal and vertical dynamics of element/Ca in the GOA

Trace element incorporation into the calcium carbonate shells of planktic foraminifera during calcification is controlled by environmental and ecological factors in the water column such as



498 temperature, salinity, pH , the carbonate system, dust and terrigenous inputs, as well as whether
499 a species harbor photosymbionts (Schiebel & Hemleben, 2017; and others). Shells of *G. ruber*
500 *albus*, *T. clarkei* ‘big’ and *T. clarkei* ‘encrusted’ from the GOA show species-specific behavior
501 and offer new insights into how these species respond to the vertical and temporal variations
502 in the water column. For most elements, the smaller *T. clarkei* specimens display higher trace
503 element ratios than the larger *G. ruber albus*, suggesting more efficient trace element
504 incorporation to the shell or implying that its habitat deeper in the water column has conditions
505 which result in higher trace element incorporation (Fig. 3). Some element ratios such as Mg/Ca ,
506 Sr/Ca , B/Ca , Na/Ca (for *G. ruber albus*) and Ba/Ca for both *G. ruber albus* and *T. clarkei*
507 ‘encrusted’, show overlap between specimens from the water column and from core-tops (Fig.
508 3), confirming the robustness of downcore-based records allowing to further consider these
509 element/ Ca recorders of the water column as paleo-proxies.

510 While water depth likely influences element/ Ca through variations in physical and
511 chemical conditions, the observed inter-chamber variability (ICV) and element/ Ca differences
512 between species cannot be attributed to any single environmental parameter. Nonetheless,
513 elements such as Al/Ca , Ti/Ca , Mn/Ca , and Fe/Ca for all species, and Mg/Ca , Sr/Ca , Na/Ca ,
514 and Ba/Ca for *G. ruber albus* alone, demonstrate consistent behavior across the water column,
515 suggesting that depth-related factors do not significantly alter calcification mechanisms. This
516 supports the use of pooled mean values for specimens over multiple sediment traps spread over
517 depths (Levy et al., 2023). Interestingly, most element/ Ca peak during water column mixing in
518 March-April 2015 for all three morphotypes analyzed here, accompanied by larger ICV (Figs.
519 4-8). Mg/Ca in *G. ruber albus* and Sr/Ca in all three species show less pronounced excursions,
520 while other trace element ratios (e.g., Co/Ca , U/Ca) exhibit more variability and more extreme
521 values (Figs. S5 and S10). These observations can reflect: i) primary calcite structure
522 alterations driven by environmental shifts and life cycle changes, ii) secondary mineralization
523 (e.g., barite, Amorphous Calcium Carbonate, ACC) (Torres et al., 2010; Evans et al., 2020 and
524 references therein), and iii) fluid inclusions within the shell structure (Gray et al., 2023).

525 All of these relationships do possibly concern the ontogenetic PF calcite, since SEM
526 imaging of GOA specimens did not reveal secondary minerals or overgrowth on shell calcite
527 (Levy et al., 2023). Moreover, the enrichment of multiple trace elements across species
528 suggests that secondary minerals are unlikely to be responsible for these trends. Discrepancies
529 between Na/Ca in plankton tow versus core-top samples in the Red Sea (Mezger et al., 2018),
530 as well as higher Na/Ca values measured by LA-ICP-MS compared to solution ICP-MS, have
531 been linked to early diagenesis of Na-enriched phases like spines, ACC, or fluid inclusions



(Gray et al., 2023). However, spines and ACC were ruled out for GOA samples, as all of the specimens had lost their spines before analysis and ACC was not detected via SEM. Given that most element/Ca in GOA shells are elevated relative to PF data from elsewhere, fluid inclusions may be a contributing factor (Gray et al., 2023). However, more research is required to investigate whether fluid inclusions are evident in PF shells from the GOA. In the absence of fluid inclusions, environmental changes, particularly during water column mixing, are considered to be the primary drivers of the observed trace element/Ca enrichments in the GOA.

5.2 Water column and sediment signal correlation: Implications to Paleooceanographic studies

Several element ratios (e.g., Al/Ca, Ti/Ca, Mn/Ca, Fe/Ca, Nd/Ca, U/Ca, Co/Ca, and Th/Ca) exhibit discrepancies between water column and core-top specimens (Fig. 3). Some, like Co/Ca, have lower values in surface sediment than the water column, while others, like Fe/Ca show higher values. Differences between sediment trap samples and core-top samples may stem from differential diagenetic processes that affect element/Ca in specimens taken from the water column and the sea floor. For example, diagenetic processes can lead to Mn accumulation and higher Mn/Ca in PF from the core top (McKenzie, 1980; Steiner et al., 2017). Conversely, core-top PF samples may show lower ratios due to the release of these metals into pore water over time (e.g., Co/Ca, Fig. 3i). This release can alter the elemental composition, potentially skewing paleoenvironmental reconstructions. Understanding these processes is crucial for accurately interpreting geochemical data from both sample types.

Despite the offsets of Al/Ca and Ti/Ca between core top and water column specimens, they nevertheless may be utilized to trace the origins of terrigenous inputs and identify periods of dust deposition in the geological record (Torfstein et al., 2017; Martinez-Garcia et al., 2011). Our data reveal significant seasonal excursions in Al/Ca and may demonstrate the use of Al/Ca and Ti/Ca in PF tests as proxies for dust or terrigenous input to the ocean (Fig. S3).

Core top element/Ca values that fall within the same range of values of the sediment trap specimens (Mg/Ca, Sr/Ca, B/Ca, Na/Ca, and Ba/Ca; Fig. 3) suggest that they could reflect water column conditions. The high temporal variability in many of these element/Ca data, together with the varying PF population dynamics throughout the year (Fig. 2) may be considered when approaching PF from sediment cores. Seasonal trends in element/Ca are often obscured by the spring mixing event. However, exceptions to this are observed in Mg/Ca for *G. ruber albus* (Fig. 4; Levy et al., 2023) and B/Ca for *T. clarkei* (Fig. 6), where clear seasonal patterns emerge. A key limitation of reconstructing past environments from element/Ca in PF



566 shells is the challenge of disentangling seasonal effects from other more episodic
567 environmental signals. However, by identifying water column mixing events through positive
568 element/Ca excursions and elevated ICV, which are evident across all three species (Figs. 4-
569 8), it may be possible to identify the time intervals over which environmental changes are
570 reconstructed. This could allow for more accurate reconstructions of shifts in temperature,
571 carbonate chemistry, and nutrient availability during specific mixing events, improving our
572 understanding of past ocean conditions.

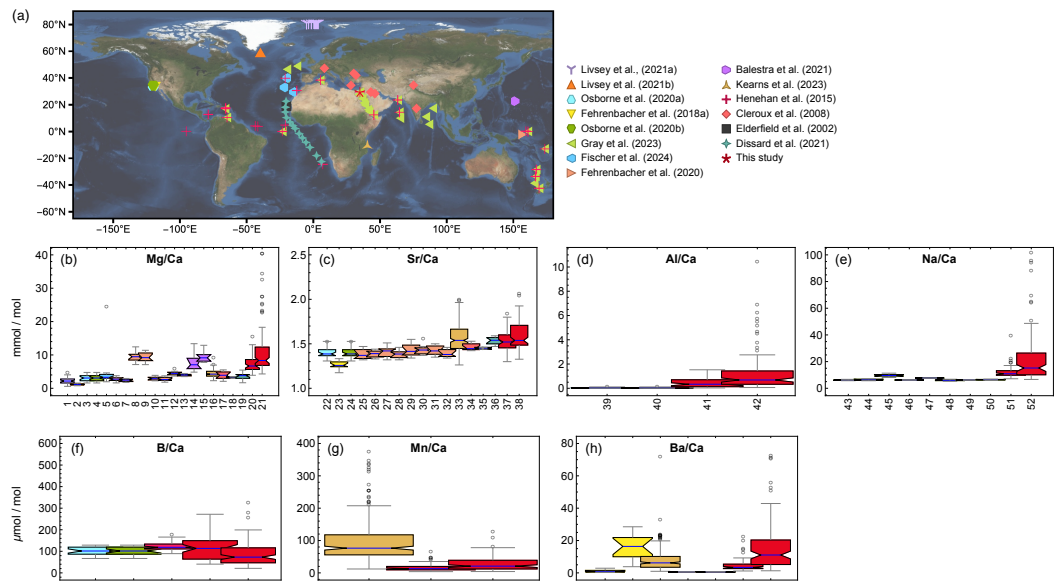
573

574 5.3 Regional comparison of geochemical conditions and PF element/Ca

575 The Mg/Ca, Al/Ca, and Na/Ca in PF from the GOA generally exceed those reported from other
576 regions (Fig. 12b – 14e). Sr/Ca values, while reaching up to 2.2 mmol/mol during spring, have
577 an average of 1.5 mmol/mol, consistent with previous studies (Fig. 12c; Kisakürek et al., 2008;
578 Cleroux et al., 2008; Elderfield et al., 2002; Brown & Elderfield, 1996; Dissard et al., 2021).
579 The high Mg/Ca range in the GOA versus typical open-ocean levels (0.5-5 $\mu\text{mol/mol}$) is
580 attributed to elevated salinity (~ 41 compared to mean ocean values of 34.7), which is also
581 evident by the high Na/Ca. The high Al/Ca values and their large variation may be attributed
582 to the close proximity of GOA to terrestrial input. Ba/Ca in the GOA are significantly higher
583 than the values reported in prior studies from Atlantic Ocean core samples and culture
584 experiments (Hönisch et al., 2011; Lea & Boyle, 1991), representing a roughly ten-fold
585 difference. These discrepancies likely stem from two factors: (1) higher salinity in the GOA
586 increases the availability of cations and trace element incorporation into foraminifera shells,
587 and (2) higher-resolution measurements here which reveal chamber-specific elemental ratios,
588 where early chambers (F-1 and F-2) exhibit higher values than final chambers, leading to more
589 accurate, chamber-level data compared to bulk measurements. Combined, these factors explain
590 the elevated values relative to global reports.



591



592

593 Figure 12. Global comparison of major and trace element-to-calcium ratios. (a) sample global
594 map, (b) Mg/Ca of *N. pachyderma*, *G. bulloides*, *G. ruber white*, *N. dutertrei*, *O. universa*, *P.*
595 *obliquiloculata*, *T. sacculifer* and *T. clarkei* derived from various sources (plankton tows/nets,
596 sediment traps, cores) and measured by Laser Ablation (LA)-ICP-MS, solution-ICP-MS (SOL)
597 and Electron micro-probe analyses (EPMA). (c) Sr/Ca of *G. bulloides*, *G. ruber white*, *N.*
598 *dutertrei*, *O. universa*, *P. obliquiloculata*, *T. sacculifer* and *T. clarkei* derived from various
599 sources (plankton tows/nets, sediment traps, cores) and measured by LA-ICP-MS and solution-
600 ICP-MS. (d) Al/Ca of *G. bulloides*, *G. ruber white* and *T. clarkei* derived from sediment traps
601 and measured by LA-ICP-MS. (e) Na/Ca of *G. ruber white* and *T. clarkei* from various sources
602 (plankton tows/nets, sediment traps, cores and cultured samples) and measured by LA-ICP-MS
603 and solution-ICP-MS. (f) B/Ca of *G. bulloides*, *G. ruber white* and *T. clarkei* derived from
604 sediment traps and measured by LA-ICP-MS. (g) Mn/Ca of *G. ruber white* and *T. clarkei*
605 derived from cores and sediment traps and measured by LA-ICP-MS. (h) Ba/Ca of *G. ruber*
606 *white*, *N. dutertrei* and *T. clarkei* derived from various sources (plankton tows/nets, sediment
607 traps, cores and cultured samples) and measured by LA-ICP-MS. See table 1 for detailed
608 description of methods.

609

610



#	Element/Ca	Reference	Species	Collecting method	Measuring method
1	Mg/Ca	Livsey et al. (2021a)	<i>N. pachyderma</i>	Plankton tows / nets	LA
2	Mg/Ca	Livsey et al. (2021b)	<i>N. pachyderma</i>	Sediment traps	LA
3	Mg/Ca	Osborne et al. (2020)	<i>G. bulloides</i>	Sediment trap	LA
4	Mg/Ca	Osborne et al. (2020b)	<i>G. bulloides</i>	Sediment trap	LA
5	Mg/Ca	Fischer et al. (2024)	<i>G. ruber</i>	Plankton tows / nets	LA
6	Mg/Ca	Fehrenbacher et al. (2020)	<i>N. dutertrei</i>	Core	LA
7	Mg/Ca	Fehrenbacher et al. 2020	<i>N. dutertrei</i>	Core	SOL
8	Mg/Ca	Fehrenbacher et al. (2020)	<i>O. universa</i>	Core	LA
9	Mg/Ca	Fehrenbacher et al. (2020)	<i>O. universa</i>	Core	SOL
10	Mg/Ca	Fehrenbacher et al. (2020)	<i>P. obliquiloculata</i>	Core	LA
11	Mg/Ca	Fehrenbacher et al. (2020)	<i>P. obliquiloculata</i>	Core	SOL
12	Mg/Ca	Fehrenbacher et al. (2020)	<i>T. sacculifer</i>	Core	LA
13	Mg/Ca	Fehrenbacher et al. (2020)	<i>T. sacculifer</i>	Core	SOL
14	Mg/Ca	Balestra et al. (2021)	<i>O. universa</i>	Plankton tows / nets	EPMA
15	Mg/Ca	Balestra et al. (2022)	<i>O. universa</i>	Plankton tows / nets	EPMA
16	Mg/Ca	Kearns et al. (2023)	<i>G. ruber</i>	Core	LA



17	Mg/Ca	Cleroux et al. (2008)	<i>G. ruber</i>	Core	SOL
18	Mg/Ca	Elderfield et al. (2002)	<i>G. ruber</i>	Core	SOL
19	Mg/Ca	Dissard et al. (2021)	<i>T. sacculifer</i>	Plankton tows / nets	LA
20	Mg/Ca	This study	<i>G. ruber</i>	Sediment trap	LA
21	Mg/Ca	This study	<i>T. clarkei</i>	Sediment trap	LA
22	Sr/Ca	Osborne et al. (2020)	<i>G. Bulloides</i>	Sediment trap	LA
23	Sr/Ca	Fehrenbacher et al. (2018a)	<i>N. dutertrei</i>	Plankton tows / nets	LA
24	Sr/Ca	Osborne et al. (2020b)	<i>G. bulloides</i>	Sediment trap	LA
25	Sr/Ca	Fehrenbacher et al. (2020)	<i>N. dutertrei</i>	Core	LA
26	Sr/Ca	Fehrenbacher et al. (2020)	<i>N. dutertrei</i>	Core	SOL
27	Sr/Ca	Fehrenbacher et al. (2020)	<i>O. universa</i>	Core	LA
28	Sr/Ca	Fehrenbacher et al. (2020)	<i>O. universa</i>	Core	SOL
29	Sr/Ca	Fehrenbacher et al. (2020)	<i>P. obliquiloculata</i>	Core	LA
30	Sr/Ca	Fehrenbacher et al. (2020)	<i>P. obliquiloculata</i>	Core	SOL
31	Sr/Ca	Fehrenbacher et al. (2020)	<i>T. sacculifer</i>	Core	LA
32	Sr/Ca	Fehrenbacher et al. (2020)	<i>T. sacculifer</i>	Core	SOL
33	Sr/Ca	Kearns et al. (2023)	<i>G. ruber</i>	Core	LA
34	Sr/Ca	Cleroux et al. (2008)	<i>G. ruber</i>	Core	SOL



35	Sr/Ca	Elderfield et al. (2002)	<i>G. ruber</i>	Core	SOL
36	Sr/Ca	Dissard et al. (2021)	<i>T. sacculifer</i>	Plankton tows / nets	LA
37	Sr/Ca	This study	<i>G. ruber</i>	Sediment trap	LA
38	Sr/Ca	This study	<i>T. clarkei</i>	Sediment trap	LA
39	Al/Ca	Osborne et al. (2020)	<i>G. Bulloides</i>	Sediment trap	LA
40	Al/Ca	Osborne et al. (2020b)	<i>G. bulloides</i>	Sediment trap	LA
41	Al/Ca	This study	<i>G. ruber</i>	Sediment trap	LA
42	Al/Ca	This study	<i>T. clarkei</i>	Sediment trap	LA
43	Na/Ca	Gray et al. (2023)	<i>G. ruber</i>	Core	SOL
44	Na/Ca	Gray et al. (2023)	<i>G. ruber</i>	Cultured	SOL
45	Na/Ca	Gray et al. (2023)	<i>G. ruber</i>	Plankton tows / nets	LA
46	Na/Ca	Gray et al. (2023)	<i>G. ruber</i>	Plankton tows / nets	SOL
47	Na/Ca	Gray et al. (2023)	<i>G. ruber</i>	Sediment trap	LA
48	Na/Ca	Gray et al. (2023)	<i>G. ruber</i>	Sediment trap	SOL
49	Na/Ca	Gray et al. (2023)	<i>G. ruber mixed</i>	Core	SOL
50	Na/Ca	Gray et al. (2023)	<i>G. ruber sl</i>	Core	SOL
51	Na/Ca	This study	<i>G. ruber</i>	Sediment trap	LA
52	Na/Ca	This study	<i>T. clarkei</i>	Sediment trap	LA



53	B/Ca	Osborne et al. (2020)	<i>G. Bulloides</i>	Sediment trap	LA
54	B/Ca	Osborne et al. (2020b)	<i>G. Bulloides</i>	Sediment trap	LA
55	B/Ca	Henehan et al. (2015)	<i>G. ruber</i>	Core	SOL
56	B/Ca	This study	<i>G. ruber</i>	Sediment trap	LA
57	B/Ca	This study	<i>T. clarkei</i>	Sediment trap	LA
58	Mn/Ca	Kearns et al. (2023)	<i>G. ruber</i>	Core	LA
59	Mn/Ca	This study	<i>G. ruber</i>	Sediment trap	LA
60	Mn/Ca	This study	<i>T. clarkei</i>	Sediment trap	LA
61	Ba/Ca	Fehrenbacher et al. (2018a)	<i>N. dutertrei</i>	Cultured	LA
62	Ba/Ca	Fehrenbacher et al. (2018a)	<i>N. dutertrei</i>	Plankton tows / nets	LA
63	Ba/Ca	Kearns et al. (2023)	<i>G. ruber</i>	Core	LA
64	Ba/Ca	Hönisch et al. (2011)	<i>G. bulloides</i>	Cultured	SOL
65	Ba/Ca	Hönisch et al. (2011)	<i>O. universa</i>	Cultured	SOL
66	Ba/Ca	This study	<i>G. ruber</i>	Sediment trap	LA
67	Ba/Ca	This study	<i>T. clarkei</i>	Sediment trap	LA

611

612 Table 1: detailed description of the different species, measurement methods and sample
613 origin used for the compilation in figure 12. LA stands for Laser Ablation (LA)-ICP-MS,
614 SOL is solution-ICP-MS and EPMA is Electron micro-probe analyses.

615

616 6. Summary and conclusions:



We investigated the effects of inter-chamber variability on the proxy systematics in the hyper saline oligotrophic GOA using single chamber LA ICP-MS analysis measured on two flux-dominating planktic foraminifer (PF) species *G. ruber albus* and *T. clarkei* with its two phenotypes ‘big’ and ‘encrusted’. We observed how element/Ca varies in PF chambers as a function of environmental changes in order to then be used as proxies for past oceanic and climatic reconstruction. The results show that some element/Ca exhibit temporal and seasonal variations related to environmental conditions in the water column such as Mg/Ca in *G. ruber albus* as a temperature proxy, and B/Ca in *T. clarkei* as a proxy of pH. Although other element/Ca values display more limited variability (e.g., Na/Ca) they may still be of use as paleo-proxies when combined in global calibration studies.

Water column mixing has been shown to have a significant effect of element/Ca positive excursions in the analyzed *G. ruber albus*, and two *T. clarkei* morphotypes, which may limit the use of some element ratios as proxies, or alternatively, be used as a proxy for water column mixing. Generally, pooled-mean values of element/Ca in the PF tests in the GOA are species-specific and element-specific, and are elevated compared to other regions (e.g., Mg/Ca, Al/Ca, Na/Ca). However, the final chamber F0 is different in comparison to the preceding chambers F-1 and F-2, suggesting that the element composition of F0 may be biased and unreliable in terms of recording environmental conditions.

Our findings indicate that high-resolution analytical techniques, such as LA ICP-MS enable studying single chamber compositions and variations. Although pooled mean values of specimens over various water depths are recommended for their incorporation as proxies, ICP-MS can also be used as a tracer of environmental factors. Exploring different biochemical or physiological mechanisms which are responsible for the element/Ca variations between species and chambers are critical to shed light on how element/Ca are incorporated to the PF shells. Despite these limitations, the results provide valuable insights into the complex behavior of element/Ca in PF shells.

Data availability

Tabular supplementary data generated in this study can be found at PANGAEA (DOI: *will be added following acceptance*).

Author contributions



648 NL, AT, and RS designed the study; NL, BS, UW, and KPJ, performed the measurements;
649 NL, NC, AT, and RS analyzed the data; NL, RS and AT wrote the manuscript draft; NL, RS,
650 AT and GH reviewed and edited the manuscript.

651

652 The authors declare that they have no conflict of interest.

653

654 Acknowledgments

655 We wish to acknowledge the IUI marine crew and B. Yarden for their assistance in field work
656 and sample handling. The National Monitoring Program are thanked for their support and
657 sharing results and E. Levy for fruitful discussions. We are thankful for the three anonymous
658 reviewers whom their comments significantly improved this manuscript. This work was
659 supported by Israel Science Foundation grant 834/19 (to AT), a Minerva PhD Fellowship
660 stipend (to NL) and a scholarship from the Advance School for Environmental Studies, HUJI
661 (to NL).

662

663



664 References

665 Allen, K. A., Hönlisch, B., Eggins, S. M., Haynes, L. L., Rosenthal, Y., & Yu, J. Trace element
666 proxies for surface ocean conditions: A synthesis of culture calibrations with planktic
667 foraminifera. *Geochim Cosmochim Acta*, 193, 197-221. (2016).

668

669 Allen, K. A., Hönlisch, B., Eggins, S. M., Yu, J., Spero, H. J., & Elderfield, H. Controls on
670 boron incorporation in cultured tests of the planktic foraminifer *Orbulina universa*. *Earth
671 Planet Sc Lett*, 309(3-4), 291-301. (2011).

672

673 Allen, K. A., Hönlisch, B., Eggins, S. M., & Rosenthal, Y. Environmental controls on B/Ca in
674 calcite tests of the tropical planktic foraminifer species *Globigerinoides ruber* and
675 *Globigerinoides sacculifer*. *Earth Planet Sc Lett*, 351, 270-280. (2012).

676

677 Anderson, R. F., Bacon, M. P., & Brewer, P. G. Removal of ^{230}Th and ^{231}Pa from the open
678 ocean. *Earth Planet Sc Lett*, 62(1), 7-23. (1983).

679

680 Babila, T. L., Rosenthal, Y., & Conte, M. H. Evaluation of the biogeochemical controls on
681 B/Ca of *Globigerinoides ruber* white from the Oceanic Flux Program, Bermuda. *Earth Planet
682 Sc Lett*, 404, 67-76. (2014).

683

684 Balestra, B., Rose, T., Fehrenbacher, J., Knobelspiesse, K. D., Huber, B. T., Gooding, T., &
685 Paytan, A. In Situ Mg/Ca Measurements on Foraminifera: Comparison Between Laser
686 Ablation Inductively Coupled Plasma Mass Spectrometry and Wavelength-Dispersive X-Ray
687 Spectroscopy by Electron Probe Microanalyzer. *Geochem Geophys Geosy*, 22(2),
688 e2020GC009449. (2021).

689

690 Bé, A. W., Hemleben, C., Anderson, O. R., Spindler, M., Hacunda, J., & Tuntivate-Choy, S.
691 Laboratory and field observations of living planktonic foraminifera. *Micropaleontology*, 155-
692 179. (1977).

693

694 Beasley, C., Kender, S., Giosan, L., Bolton, C. T., Anand, P., Leng, M. J., Nilsson-Kerr k.,
695 Ullmann C. V., Hesselbo S. P., & Littler, K. Evidence of a South Asian proto-monsoon during
696 the Oligocene-Miocene transition. *Paleoceanogr Paleoclimatol*, 36(9), e2021PA004278.
697 (2021).



- 698 Berggren, W. A., Kent, D. V., Swisher, C. C., & Aubry, M. P. A revised Cenozoic
699 geochronology and chronostratigraphy. (1995).
700
- 701 Bertlich, J., Nürnberg, D., Hathorne, E. C., De Nooijer, L. J., Mezger, E. M., Kienast, M.,
702 Nordhausen S., Reichart G., Schönfeld J., & Bijma, J. Salinity control on Na incorporation into
703 calcite tests of the planktonic foraminifera *Trilobatus sacculifer*—evidence from culture
704 experiments and surface sediments. *Biogeosciences*, 15(20), 5991-6018. (2018).
705
- 706 Bolton, A., Baker, J. A., Dunbar, G. B., Carter, L., Smith, E. G., & Neil, H. L. Environmental
707 versus biological controls on Mg/Ca variability in *Globigerinoides ruber* (white) from core top
708 and plankton tow samples in the southwest Pacific Ocean. *Paleoceanography*, 26(2). (2011).
- 709 Brummer, G. J. A., & Kučera, M. Taxonomic review of living planktonic foraminifera. *J*
710 *Micropalaeontol*, 41(1), 29-74. (2022).
- 711 Brown, S. J., & Elderfield, H. Variations in Mg/Ca and Sr/Ca ratios of planktonic foraminifera
712 caused by postdepositional dissolution: Evidence of shallow Mg-dependent
713 dissolution. *Paleoceanography*, 11(5), 543-551. (1996).
714
- 715 Chang, F., Li, T., Xiong, Z., & Xu, Z. Evidence for sea level and monsoonally driven variations
716 in terrigenous input to the northern East China Sea during the last 24.3
717 ka. *Paleoceanography*, 30(6), 642-658. (2015).
718
- 719 Chase, Z., Paytan, A., Beck, A., Biller, D., Bruland, K., Measures, C., & Sañudo-Wilhelmy, S.
720 Evaluating the impact of atmospheric deposition on dissolved trace-metals in the Gulf of
721 Aqaba, Red Sea. *Mar Chem*, 126(1-4), 256-268. (2011).
722
- 723 Chernihovsky, N., Torfstein, A., & Almogi-Labin, A. Seasonal flux patterns of planktonic
724 foraminifera in a deep, oligotrophic, marginal sea: Sediment trap time series from the Gulf of
725 Aqaba, northern Red Sea. *Deep-Sea Res Pt I*, 140, 78-94. (2018).
726
- 727 Chernihovsky, N., Almogi-Labin, A., Kienast, S. S., & Torfstein, A. The daily resolved
728 temperature dependence and structure of planktonic foraminifera blooms. *Sci Rep-Uk*, 10(1),
729 17456. (2020).



730
731 Cléroux, C., Cortijo, E., Anand, P., Labeyrie, L., Bassinot, F., Caillon, N., & Duplessy, J. C.
732 Mg/Ca and Sr/Ca ratios in planktonic foraminifera: Proxies for upper water column
733 temperature reconstruction. *Paleoceanography*, 23(3). (2008).
734
735 Costa, K. M., Hayes, C. T., Anderson, R. F., Pavia, F. J., Bausch, A., Deng, F., Dutay, J.,
736 Geibert, W. Heinze, C., Henderson, G., Hillaire-Marcel, C., Hoffmann, S., Jaccard, S. L.,
737 Jacobel, A. W., Kienast, S. S., Kipp, L., Lerner, P., Lippold, J., Lund, D., Marcantonio, F.,
738 McGee, D., McManus, J. F., Mekik, F., Middleton, J. L., Missiaen, L., Not, C., Pichat, S.,
739 Robinson, L. F., Rowland, G. H., Roy-Barman, M., Tagliabue, A., Torfstein, A., Winckler, G.,
740 & Zhou, Y. 230Th normalization: New insights on an essential tool for quantifying sedimentary
741 fluxes in the modern and Quaternary ocean. *Paleoceanogr Paleoclimatol*, 35(2),
742 e2019PA003820. (2020).
743
744 Davis, C. V., Fehrenbacher, J. S., Benitez-Nelson, C., & Thunell, R. C. Trace element
745 heterogeneity across individual planktic foraminifera from the Modern Cariaco Basin. *J*
746 *Foramin Res*, 50(2), 204-218. (2020).
747
748 Dissard, D., Reichart, G. J., Menkes, C., Mangeas, M., Frickenhaus, S., & Bijma, J. Mg/Ca,
749 Sr/Ca and stable isotopes from the planktonic foraminifera *T. sacculifer*: testing a multi-proxy
750 approach for inferring paleotemperature and paleosalinity. *Biogeosciences*, 18(2), 423-439.
751 (2021).
752
753 Elderfield, H., Vautravers, M., & Cooper, M. The relationship between shell size and Mg/Ca,
754 Sr/Ca, $\delta^{18}\text{O}$, and $\delta^{13}\text{C}$ of species of planktonic foraminifera. *Geochem Geophys Geosy*, 3(8),
755 1-13. (2002).

756 Evans, D., Gray, W. R., Rae, J. W., Greenop, R., Webb, P. B., Penkman, K., Kröger, R., &
757 Allison, N. Trace and major element incorporation into amorphous calcium carbonate (ACC)
758 precipitated from seawater. *Geochim Cosmochim Ac*, 290, 293-311. (2020).
759



- 760 Fehrenbacher, J., Marchitto, T., & Spero, H. J. Comparison of Laser Ablation and Solution-
761 Based ICP-MS Results for Individual Foraminifer Mg/Ca and Sr/Ca Analyses. *Geochem*
762 *Geophys Geosy*, 21(12), e2020GC009254. (2020).
763
- 764 Fehrenbacher, Jennifer; Russell, Ann D; Davis, Catherine V; Spero, Howard J; Chu, Edward;
765 Hönisch, Bärbel: Average barium/calcium ratios of cultured foraminifer specimens of
766 Neoglobobulimina dutertrei, listed by experiment
767 [dataset]. PANGAEA, <https://doi.org/10.1594/PANGAEA.895792>, (2018).
768
- 769 Fischer, A., Schiebel, R., Jochum, K. P., Heins, L., Arns, A. I., Aardema, H. M., Slagter, H.,
770 Calleja, M. L., Levy, N., Stoll, B., Weis, U., Repschläger, J., & Haug, G. H. Single chamber
771 Mg/Ca analyses of Globigerinoides ruber for paleo-proxy calibration using femtosecond LA-
772 ICP-MS. *Sci. Data*, 11(1), 583. (2024).
773
- 774 Francois, R., Frank, M., Rutgers van der Loeff, M. M., & Bacon, M. P. 230Th normalization:
775 An essential tool for interpreting sedimentary fluxes during the late
776 Quaternary. *Paleoceanography*, 19(1). (2004).
777
- 778 Fritz-Endres, T., Fehrenbacher, J. S., Russell, A. D., & Cynar, H. Increased productivity in the
779 equatorial pacific during the deglaciation inferred from the Ba/Ca ratios of non-spinose
780 planktic foraminifera. *Paleoceanogr Paleoclimatol*, 37(12), e2022PA004506. (2022).
781
- 782 Ganor, E., & Foner, H. A. Mineral dust concentrations, deposition fluxes and deposition
783 velocities in dust episodes over Israel. *J Geophys Res-Atmos*, 106(D16), 18431-18437. (2001).
784
- 785 Ganssen, G. M., Peeters, F. J. C., Metcalfe, B., Anand, P., Jung, S. J. A., Kroon, D., &
786 Brummer, G. J. Quantifying sea surface temperature ranges of the Arabian Sea for the past 20
787 000 years. *Clim Past*, 7(4), 1337-1349. (2011).
788
- 789 Geerken, E., De Nooijer, L. J., van Dijk, I., & Reichert, G. J. Impact of salinity on element
790 incorporation in two benthic foraminiferal species with contrasting magnesium
791 contents. *Biogeosciences*, 15(7), 2205-2218. (2018).



- 792
- 793 Gray, W. R., Evans, D., Henehan, M., Weldeab, S., Lea, D. W., Müller, W., & Rosenthal, Y.
794 Sodium incorporation in foraminiferal calcite: An evaluation of the Na/Ca salinity proxy and
795 evidence for multiple Na-bearing phases. *Geochim Cosmochim Acta*, 348, 152-164. (2023).
- 796
- 797 Gupta, B. K. S. *Modern foraminifera* (pp. 7-36). B. K. S. Gupta (Ed.). Dordrecht: Kluwer
798 Academic Publishers. (1999).
- 799 Haug, G. H., Gunther, D., Peterson, L. C., Sigman, D. M., Hughen, K. A., & Aeschlimann, B.
800 Climate and the collapse of Maya civilization. *Science*, 299(5613), 1731-1735. (2003).
- 801 Haynes, L. L., Hönisch, B., Holland, K., Rosenthal, Y., & Eggins, S. M. Evaluating the planktic
802 foraminiferal B/Ca proxy for application to deep time paleoceanography. *Earth Planet Sc*
803 *Lett*, 528, 115824. (2019).
- 804 Henehan, M. J., Foster, G. L., Rae, J. W., Prentice, K. C., Erez, J., Bostock, H. C., Marshall,
805 B. J., & Wilson, P. A. Evaluating the utility of B/Ca ratios in planktic foraminifera as a proxy
806 for the carbonate system: A case study of *Globigerinoides ruber*. *Geochem Geophys*
807 *Geosy*, 16(4), 1052-1069. (2015).
- 808 Hönisch, B., Allen, K. A., Russell, A. D., Eggins, S. M., Bijma, J., Spero, H. J., Lea, D. W., &
809 Yu, J. Planktic foraminifera as recorders of seawater Ba/Ca. *Mar Micropaleontol*, 79(1-2), 52-
810 57. (2011).
- 811 Hönisch, B., Fish, C. R., Phelps, S. R., Haynes, L. L., Dyez, K., Holland, K., Fehrenbacher, J.,
812 Allen, K. A., Eggins, S. M., & Goes, J. I. Symbiont photosynthesis and its effect on boron
813 proxies in planktic foraminifera. *Paleoceanogr Paleoclimatol*, 36(10), e2020PA004022.
814 (2021).
- 815 Hupp, B. N., & Fehrenbacher, J. S. Intratest trace element variability in polar and subpolar
816 planktic foraminifera: Insights into vital effects, ontogeny, and biomineralization processes. *J*
817 *Foramin Res*, 54(4), 355-374. (2024).
- 818 Israel National Monitoring Program (NMP) ([http://www.iui-eilat.ac.](http://www.iui-eilat.ac.il/Research/NMPmeteodata.aspx)
819 [il/Research/NMPmeteodata.aspx](http://www.iui-eilat.ac.il/Research/NMPmeteodata.aspx); Shaked and Genin. (2016).



- 820 Jochum, K. P., Jentzen, A., Schiebel, R., Stoll, B., Weis, U., Leitner, J., Repschläger, J.,
821 Nürnberg, D., & Haug, G. H. High-resolution Mg/Ca measurements of foraminifer shells using
822 femtosecond LA-ICP-MS for paleoclimate proxy development. *Geochem Geophys*
823 *Geosy*, 20(4), 2053-2063. (2019).
- 824
- 825 Jochum, K. P., Stoll, B., Weis, U., Jacob, D. E., Mertz-Kraus, R., & Andreae, M. O. Non-
826 matrix-matched calibration for the multi-element analysis of geological and environmental
827 samples using 200 nm femtosecond LA-ICP-MS: A comparison with nanosecond
828 lasers. *Geostand Geoanal Res*, 38(3), 265-292. (2014).
- 829
- 830 Jonkers, L., De Nooijer, L. J., Reichart, G. J., Zahn, R., & Brummer, G. J. Encrustation and
831 trace element composition of *Neoglobobulimina dutertrei* assessed from single chamber
832 analyses—implications for paleotemperature estimates. *Biogeosciences*, 9(11), 4851-4860.
833 (2012).
- 834
- 835 Katz, M. E., Cramer, B. S., Franzese, A., Hönisch, B., Miller, K. G., Rosenthal, Y., & Wright,
836 J. D. Traditional and emerging geochemical proxies in foraminifera. *J Foramin Res*, 40(2),
837 165-192. (2010).
- 838
- 839 Katz, T., Ginat, H., Eyal, G., Steiner, Z., Braun, Y., Shalev, S., & Goodman-Tchernov, B. N.
840 Desert flash floods form hyperpycnal flows in the coral-rich Gulf of Aqaba, Red Sea. *Earth*
841 *Planet Sc Lett*, 417, 87-98. (2015).
- 842
- 843 Kearns, L. E., Searle-Barnes, A., Foster, G. L., Milton, J. A., Standish, C. D., & Ezard, T. H.
844 G. The influence of geochemical variation among *Globigerinoides ruber* individuals on
845 Paleooceanographic reconstructions. *Paleoceanogr Paleoclimatol*, 38(4), e2022PA004549.
846 (2023).
- 847
- 848 Kısakürek, B., Eisenhauer, A., Böhm, F., Garbe-Schönberg, D., & Erez, J. Controls on shell
849 Mg/Ca and Sr/Ca in cultured planktonic foraminifera, *Globigerinoides ruber* (white). *Earth*
850 *Planet Sc Lett*, 273(3-4), 260-269. (2008).
- 851



- 852 Kucera, M. Chapter six planktonic foraminifera as tracers of past oceanic
853 environments. Editor(s): Claude Hillaire-Marcel, Anne De Vernal, *Developments in marine*
854 *geology*, Elsevier, 1, 213-262. ISBN 9780444527554, (2007).
855
- 856 Lea, D. W., & Boyle, E. A. Barium in planktonic foraminifera. *Geochim Cosmochim*
857 *Ac*, 55(11), 3321-3331. (1991).
858
- 859 Levy, N., Torfstein, A., Schiebel, R., Chernihovsky, N., Jochum, K. P., Weis, U., Stoll, B., &
860 Haug, G. H. Temperature calibration of elevated Mg/Ca in planktic Foraminifera shells from
861 the hypersaline Gulf of Aqaba. *Geochem Geophys Geosy*, 24(7), e2022GC010742. (2023).
862
- 863 Livsey, Caitlin M; Kozdon, Reinhard; Bauch, Dorothea; Brummer, Geert-Jan A; Jonkers,
864 Lukas; Orland, Ian; Hill, Tessa M; Spero, Howard J: In situ Magnesium/Calcium analyses by
865 LA-ICP-MS in individual *N. pachyderma* shells from plankton tows deployed in the Fram
866 Strait [dataset]. PANGAEA, <https://doi.org/10.1594/PANGAEA.935527>, (2021a).
867
- 868 Livsey, Caitlin M; Kozdon, Reinhard; Bauch, Dorothea; Brummer, Geert-Jan A; Jonkers,
869 Lukas; Orland, Ian; Hill, Tessa M; Spero, Howard J: Mg/Ca analyses by LA-ICP-MS in *N.*
870 *pachyderma* shells from Irminger Sea sediment traps
871 [dataset]. PANGAEA, <https://doi.org/10.1594/PANGAEA.935595>, (2021b).
872
- 873 Martínez-García, A., Rosell-Melé, A., Jaccard, S. L., Geibert, W., Sigman, D. M., & Haug, G.
874 H. Southern Ocean dust–climate coupling over the past four million years. *Nature*, 476(7360),
875 312-315. (2011).
876
- 877 McKenzie, R. M. The adsorption of lead and other heavy metals on oxides of manganese and
878 iron. *Soil Res*, 18(1), 61-73. (1980).
879
- 880 Meeder, E., Mackey, K. R., Paytan, A., Shaked, Y., Iluz, D., Stambler, N., Rivlin, T., Post, A.
881 F., & Lazar, B. Nitrite dynamics in the open ocean clues from seasonal and diurnal
882 variations. *Mar Ecol Prog Ser*, 453, 11-26. (2012).
883
- 884 Mesa-Fernández, J. M., Martínez-Ruiz, F., Rodrigo-Gámiz, M., Jiménez-Espejo, F. J., García,
885 M., & Sierro, F. J. Paleocirculation and paleoclimate conditions in the western Mediterranean



- 886 basins over the last deglaciation: New insights from sediment composition variations. *Global*
887 *Planet Change*, 209, 103732. (2022).
- 888
- 889 Mezger, E. M., de Nooijer, L. J., Boer, W., Brummer, G. J. A., & Reichart, G. J. Salinity
890 controls on Na incorporation in Red Sea planktonic foraminifera. *Paleoceanography*, 31(12),
891 1562-1582. (2016).
- 892
- 893 Mezger, E. M., de Nooijer, L. J., Siccha, M., Brummer, G. J., Kucera, M., & Reichart, G. J.
894 Taphonomic and ontogenetic effects on Na/Ca and Mg/Ca in spinose planktonic foraminifera
895 from the Red Sea. *Geochim Geophys Geosy*, 19(11), 4174-4194. (2018).
- 896
- 897 Morard, R., Füllberg, A., Brummer, G. J. A., Greco, M., Jonkers, L., Wizemann, A., Weiner,
898 A. K. M., Darling, K., Siccha, M., Ledevin, R., Kitazato, H., de Gardiel-Thoron, T., de Varges,
899 C., & Kucera, M. Genetic and morphological divergence in the warm-water planktonic
900 foraminifera genus Globigerinoides. *PloS one*, 14(12), e0225246. (2019).
- 901 Naik, S. S., & Naidu, P. D. Boron/calcium ratios in Globigerinoides ruber from the Arabian
902 Sea: Implications for controls on boron incorporation. *Mar Micropaleontol*, 107, 1-7. (2014).
- 903 Nürnberg, D., Bijma, J., & Hemleben, C. Assessing the reliability of magnesium in
904 foraminiferal calcite as a proxy for water mass temperatures. *Geochim Cosmochim Ac*, 60(5),
905 803-814. (1996).
- 906 Osborne, Emily B; Umling, Natalie E; Bizimis, Michael; Buckley, Wayne; Sadekov, Aleksey
907 Y; Tappa, Eric; Marshall-Kesser, Brittney; Sautter, Leslie R; Thunell, Robert C: Boron to
908 calcium ratios (B/Ca) of sediment trap collected planktonic foraminifera from the Santa
909 Barbara Basin [dataset publication
910 series]. PANGAEA, <https://doi.org/10.1594/PANGAEA.91087>, (2020a).
- 911 Osborne, Emily B; Umling, Natalie E; Bizimis, Michael; Buckley, Wayne; Sadekov, Aleksey
912 Y; Tappa, Eric; Marshall-Kesser, Brittney; Sautter, Leslie R; Thunell, Robert C: Geochemistry
913 of Globigerina Bulloides in Santa Barbara Basin measured by Laser Ablation
914 [dataset]. PANGAEA, <https://doi.org/10.1594/PANGAEA.912273>, (2020b).



- 915 Rebotim, A., Voelker, A. H., Jonkers, L., Waniek, J. J., Meggers, H., Schiebel, R., Fraile, I.,
916 Schulz, M., & Kucera, M. Factors controlling the depth habitat of planktonic foraminifera in
917 the subtropical eastern North Atlantic. *Biogeosciences*, 14(4), 827-859. (2017).
- 918 Rosenthal, Y. Chapter nineteen elemental proxies for reconstructing cenozoic seawater
919 paleotemperatures from calcareous fossils. Editor(s): Claude Hillaire-Marcel, Anne De
920 Vernal, *Developments in Marine Geology*, Elsevier, 1, 765-797. ISBN 9780444527554,
921 (2007).
- 922
- 923 Rosenthal, Y., Perron-Cashman, S., Lear, C. H., Bard, E., Barker, S., Billups, K., Bryan, M.,
924 Delaney, M. L., deMenocal, P. B., Dwyer, G. S., Elderfield, H., German, C. R., Greaves, M.,
925 Lea, D. W., Marchitto, T. M. Jr., Pak, D. K., Paradis, G. L., Russell, A. D., Schneider, R. R.,
926 Scheiderich, K., Stott, L., Tachikawa, K., Tappa, E., Thunell, R., Wara, M., Weldeab, S., &
927 Wilson, P. A. Interlaboratory comparison study of Mg/Ca and Sr/Ca measurements in
928 planktonic foraminifera for paleoceanographic research. *Geochem Geophys Geosy* 5(4). (2004).
- 929
- 930 Sadekov, A., Eggins, S. M., De Deckker, P., Ninnemann, U., Kuhnt, W., & Bassinot, F. Surface
931 and subsurface seawater temperature reconstruction using Mg/Ca microanalysis of planktonic
932 foraminifera *Globigerinoides ruber*, *Globigerinoides sacculifer*, and *Pulleniatina*
933 *obliquiloculata*. *Paleoceanography*, 24(3). (2009).
- 934
- 935 Sadekov, A., Eggins, S. M., De Deckker, P., & Kroon, D. Uncertainties in seawater
936 thermometry deriving from intratest and intertest Mg/Ca variability in *Globigerinoides*
937 *ruber*. *Paleoceanography*, 23(1). (2008).
- 938
- 939 Schiebel, R., & Hemleben, C. *Planktic foraminifers in the modern ocean* (pp. 1-358). Berlin:
940 Springer. (2017).
- 941
- 942 Shaked, Y., & Genin, A. Israel National Monitoring Program at the Gulf of Eilat Annual
943 Report. (2016).
- 944
- 945 Spero, H. J., Mielke, K. M., Kalve, E. M., Lea, D. W. & Pak, D. K. Multispecies approach to
946 reconstructing eastern equatorial Pacific thermocline hydrography during the past 360 kyr.
947 *Paleoceanography*, 18, 1022 (2003).



948

949 Sprintall, J. & Tomczak, M. Evidence of the barrier layer in the surface layer of the tropics. *J*
950 *Geophys Res-Oceans*, 97(C5), 7305-7316. (1992).

951

952 Steiner, Z., Lazar, B., Torfstein, A., & Erez, J. Testing the utility of geochemical proxies for
953 paleoproductivity in oxic sedimentary marine settings of the Gulf of Aqaba, Red Sea. *Chem*
954 *Geol*, 473, 40-49. (2017).

955

956 Thirumalai, K., Richey, J. N., Quinn, T. M., & Poore, R. Z. Globigerinoides ruber morphotypes
957 in the Gulf of Mexico: A test of null hypothesis. Scientific reports, 4(1), 6018. Torfstein, A.,
958 Kienast, S. S., Yarden, B., Rivlin, A., Isaacs, S., & Shaked, Y. (2020). Bulk and export
959 production fluxes in the Gulf of Aqaba, Northern Red Sea. *ACS Earth Space Chem*, 4(8), 1461-
960 1479. (2014).

961

962 Torfstein, A., Teutsch, N., Tirosh, O., Shaked, Y., Rivlin, T., Zipori, A., Stein, M., Lazar, B.,
963 & Erel, Y. Chemical characterization of atmospheric dust from a weekly time series in the
964 north Red Sea between 2006 and 2010. *Geochim Cosmochim Acta*, 211, 373-393. (2017).

965

966 Torres, M. E., Martin, R. A., Klinkhammer, G. P., & Nesbitt, E. A. Post depositional alteration
967 of foraminiferal shells in cold seep settings: new insights from flow-through time-resolved
968 analyses of biogenic and inorganic seep carbonates. *Earth Planet Sc Lett*, 299(1-2), 10-22.
969 (2010).

970

971 Weldeab, S., Lea, D. W., Oberhaensli, H. & Schneider, R. R. Links between southwestern
972 tropical Indian Ocean SST and precipitation over southeastern Africa over the last 17 kyr.
973 *Palaeogeogr Palaeoclimatol*, 410, 1–13 (2014).

974

975 Yu, J., Elderfield, H., & Hönisch, B. B/Ca in planktonic foraminifera as a proxy for surface
976 seawater pH. *Paleoceanography*, 22(2). (2007).